ELSEVIER

Composites Science and Technology 60 (2000) 2917–2943

COMPOSITES SCIENCE AND TECHNOLOGY

www.elsevier.com/locate/compscitech

Determination of shear strength of unidirectional composite materials with the Iosipescu and 10° off-axis shear tests

G. Odegard, M. Kumosa *

Center for Advanced Materials and Structures, Department of Engineering, University of Denver, 2390 S. York, Denver, CO 80208, USA

Received 2 September 1999; received in revised form 8 June 2000; accepted 15 June 2000

Abstract

The purpose of this research was to determine the shear strength of a unidirectional carbon-fibre/epoxy composite by means of the 10° off-axis and 0° Iosipescu specimens subjected to shear. Detailed non-linear finite-element computations of these two tests were conducted, taking into account the actual non-linear material behavior of the composite. The tests were compared in terms of stresses and strains at failure. It was found that the shear strength of the composite can be very accurately determined by using the two independent testing techniques only if fully non-linear finite element computations of the tests are performed. The stresses and strains at failure in the 10° off-axis specimen closely match the stresses and strains at the onset of intralaminar damage near the roots of the notches in Iosipescu specimens. Owing to the difficulties associated with the measurement of the shear strength of the composite using the Iosipescu test, and in particular, with the interpretation of the experimental data, this test was found to be almost impractical for the determination of shear strength. The test can only be used if fully non-linear finite element computations of uncracked and axially cracked Iosipescu specimens are conducted in conjunction with the continuous monitoring of intralaminar damage near the roots of the notches during testing. In addition, the shear strength results obtained from the Iosipescu specimen should be independently verified by using another method, such as the 10° off-axis test.

Keywords: Shear strength; Iosipescu test; 10° off axis test

1. Introduction

The determination of the intralaminar shear strength of unidirectional polymer-matrix composites is not straight-forward. This is a result of the difficulty of subjecting a unidirectional composite material to a pure and uniform shear stress state while avoiding complications caused by machining, high costs, and the effect of other stresses. Over the years, many test methods have been devised for the characterization of the shear strength of composite materials, each with its own limitations. Among these methods are the Iosipescu, torsional tube, slotted tensile, ±45° tensile, two-rail, cross-beam sandwich, picture-frame panel, Arcan, and 10° off-axis shear tests. Perhaps the two most popular of these methods are the Iosipescu and the 10° off-axis shear test methods. The popularity of these tests is mostly a result of to the relative ease of specimen fabrication and testing, low cost, and accuracy of shear strength values [1–4].

The Iosipescu shear test was first developed by Iosipescu [5] and was subsequently applied to unidirectional composites by Adams and Walrath [6–8] and Walrath and Adams [9]. In 1993, it became an ASTM standard (ASTM D 5379-93). The Iosipescu shear test consists of a V-notched specimen mounted in both sides of the Iosipescu test fixture (Fig. 1). One side of the fixture is displaced vertically while the other side remains stationary, and opposing force couples prevent in-plane bending of the specimen. The original belief was that a state of uniform shear stress would exist in the test section between the notches [5]. However, researchers have since shown that non-uniform normal and shear stresses exist in the test section of the specimen, and stress concentrations exist at the notch tips [7,8,10–17].

The most common fiber orientation in the Iosipescu shear test for determination of intralaminar shear strength and shear modulus is the 0° fiber arrangement,

* Corresponding author. Tel.: +1-303-871-3807; fax: +1-303-871-4450.

E-mail address: mkumosa@du.edu (M. Kumosa).

0266-3538/00/$ - see front matter
PII: S0266-3538(00)00141-X

which is indicated in Fig. 1. When loaded, the first observable failure is notch-root splitting which starts near the notch-roots and propagates away from the inner loading blocks along the fibers (damage 1 in Fig. 2). The splitting is predominantly a consequence of transverse tension near the notch-roots, and it has been shown that the splits create a more uniform stress distribution along the notch-root axis [13,15,17]. At about the same time as the formation of the notch-root splits, damage starts to accumulate at the notch-roots (intralaminar damage modes 2 and 3 in Fig. 2) or at the inside tips of the inner loading blocks (mode 4 in Fig. 2). The damage (crushing) caused by the loading blocks can be significant at higher loads and may affect the shear-strength determination, not only for unidirectional composites but also for fabric-reinforced composites. Two examples of damage in the gage sections of unidirectional Iosipescu specimens are in carbon-fibre/PEEK [11] and glass/polyester [13] specimens, presented in Figs. 3 and 4, respectively.

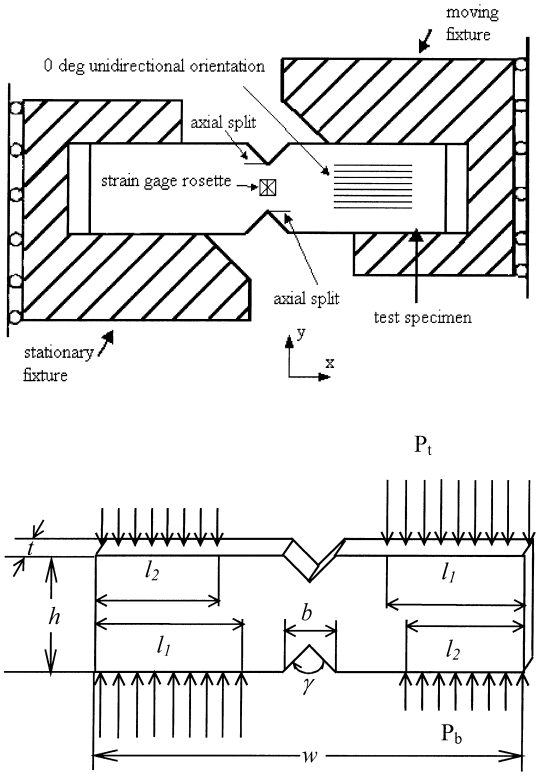

Fig. 1. The modified Wyoming Iosipescu shear test.

When unidirectional 0° composites are tested by using the Iosipescu shear method significant non-linear effects in load/displacement and load/strain diagrams are observed, especially at higher loads [15]. The most dominant factors which are responsible for the non-linear behavior of the composites investigated by the use of the Iosipescu test method are:

- specimen sliding within the fixture,
- geometric non-linearity,
- plasticity of the polymer matrix,
- damage caused by crushing,
- intralaminar damage in the gage section after the formation of the axial splits.

Since 1994, a series of papers has outlined the non-linear effects in the Iosipescu shear test that affect the shear strength determination. Ho et al.[12] showed the effects of geometric, boundary contact, and material non-linearities by using non-linear finite-element techniques. However, they determined the boundary contact and material non-linearities of unidirectional composites on the basis of a non-experimental parametric study, which lead to questionable results. Kumosa and Han [18] and Odegard et al. [16] investigated the effect of boundary contact and geometric non-linearities involved in the Iosipescu shear test. In particular, Odegard and Kumosa [15] investigated the combined effect of material, geometric and boundary contact non-linearities on the mechanical behavior of a unidirectional

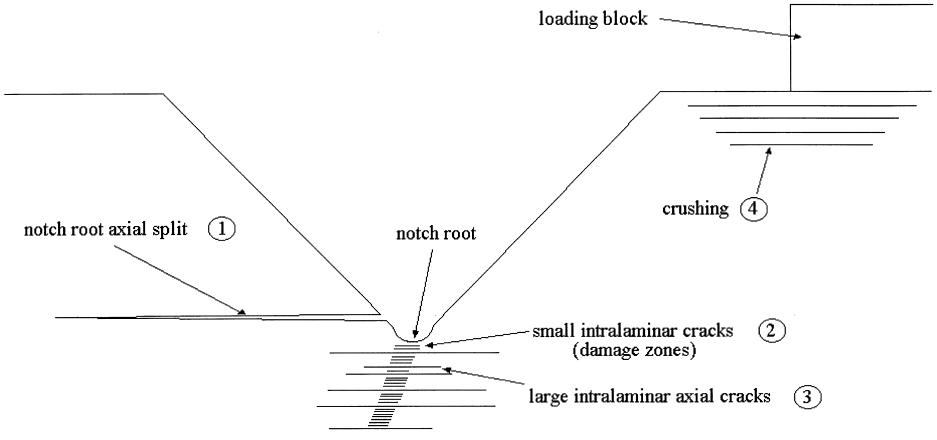

Fig. 2. Modes of failure in the Iosipescu shear test.

carbon-fibre/epoxy composite subjected to the Iosipescu test. They showed that the Iosipescu specimen response in terms of the load/displacement and load/strain diagrams can be determined accurately only if the actual elastic/plastic properties of a unidirectional composite are experimentally obtained and then used in a finite-element model. However, the effects of crushing and intralaminar damage on the global mechanical response of unidirectional 0° Iosipescu specimens has not yet been considered in finite-element computations.

The off-axis tensile test has been a fundamental method of characterizing the mechanical response of unidirectional composite materials for many years. Chamis and Sinclair [19] proposed the use of the 10° off-axis tensile test for the determination of the intralaminar shear strength of composite materials. The unidirectional fibers are oriented at $+10°$ to the loading axis (Fig. 5) which creates a stress state that will cause the material to fail mostly by shear as determined from

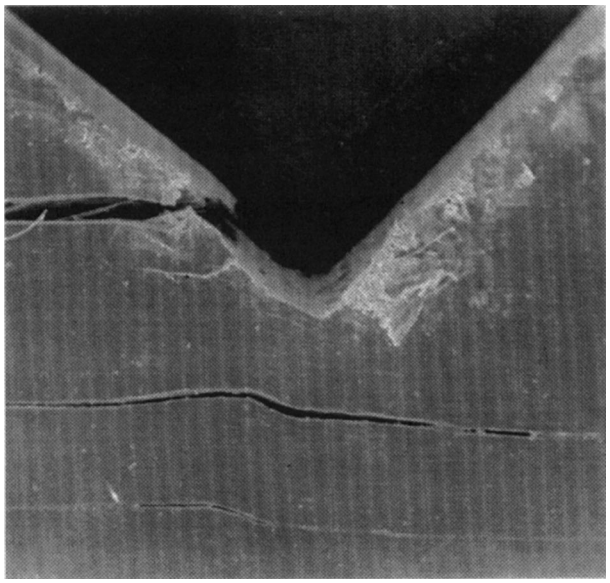

Fig. 3. Photograph of a tested graphite/PEEK Iosipescu specimen.

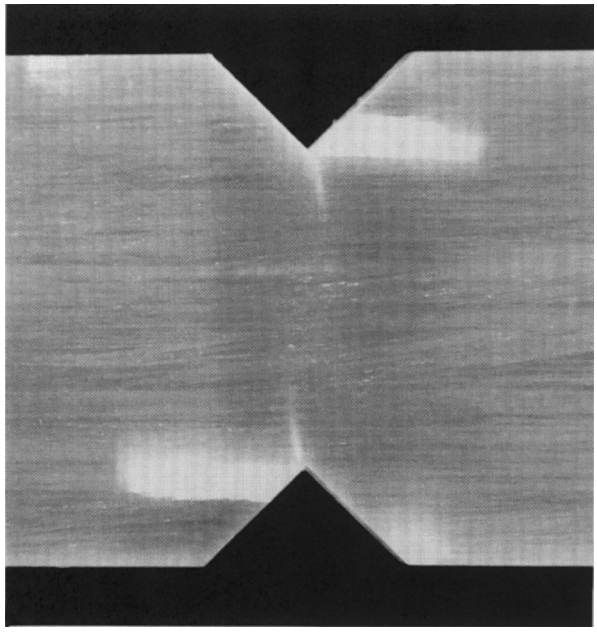

Fig. 4. Photograph of a tested glass-fibre/polyester Iosipescu specimen.

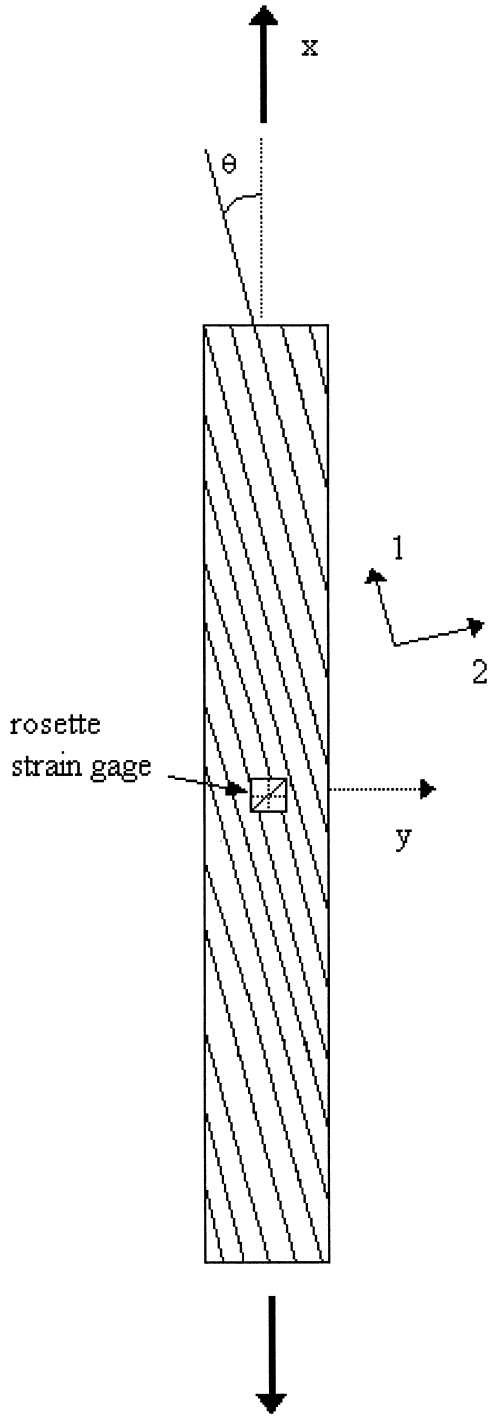

Fig. 5. The 10° off-axis test with the material and global coordinates shown.

a combined stress-failure criterion. There is currently no ASTM standard for the 10° off-axis test specifically, although ASTM D 3039-76 is a standard test method for off-axis tests on composite materials in general.

Pindera and Herakovich [20] examined the errors in the measured values of elastic properties due to the end-constraint effects. Traditionally, the specimen is gripped by straight-edged tabs, which produce parasitic shear stresses near the tab/specimen interfaces. Pierron and Vautrin [3] suggested the use of oblique tabs developed by Sun and Chung [21] to reduce these errors by providing a more uniform displacement field in the specimen. However, Balakrishnan et al. [22] performed the 10° off-axis test on a unidirectional carbon-fibre/epoxy composite with straight tabs and found that more than half of the specimens failed in the test section (instead of the gripped section), which indicated that the parasitic shear stresses were relatively small and possibly negligible. ASTM standard D 3039-76 suggests using tabs made of a material similar to that being tested in order to reduce stress concentrations. The problem with using cross-ply composite materials based on brittle matrices for the tabs, as suggested by the standard, is that their brittle nature makes gripping difficult. Most likely, the largest source of error in the 10° off-axis test is premature failure as a result of inadequate machining, especially for very brittle unidirectional composite materials. If the specimens are not carefully machined, then micro-cracks can form at the edges of the specimen, therefore significantly reducing the measured shear strength.

What has not yet been correctly addressed is the question of how the intralaminar shear strength can be properly determined from the Iosipescu and 10° off-axis tests so that similar values are obtained when testing the same composite material (intralaminar shear strength is a material property and should not change from test to test). A single criterion based on either stresses or strains should be able to predict the same shear strength of a particular composite using either test. This criterion can only be determined if the proper elastic/plastic properties of a particular composite material are known so that an accurate finite-element analysis can determine the internal stresses and strains at the points where failure occurs. In this paper, the time-independent elastic/plastic properties of a unidirectional carbon-fibre/epoxy composite (Ciba-Geigy XAS-914) are determined and used to calculate numerically the stresses and strains in both 0° Iosipescu and 10° off-axis tensile specimens.

2. Plasticity model

Many researchers have developed macro-mechanical time-independent plasticity models for unidirectional polymer-matrix composite materials. Hill's model [23] was originally developed for anisotropic cold-rolled metals. Griffin et al. [24] and Spencer [25] used approaches similar to that of Hill for modeling the non-linear behavior of unidirectional composites. Sun and Chen [26] proposed a simple single-parameter plasticity model to describe the nonlinear transverse tension and shear behavior of composite materials. All of these approaches assume a relationship between an effective stress and effective plastic strain. This is an important assumption in the plasticity of isotropic materials, and has shown some promise in modeling the plasticity of anisotropic materials. However, it may be an over-restrictive assumption when applied to polymer-matrix composite materials since they exhibit drastically different modes of failure under different load paths. Hansen et al. [27] proposed an invariant-based flow rule which incorporates a scalar hardening parameter that allows the hardening to be determined as a function of the load path, and not an effective-stress/plastic-strain relationship. Some research has suggested that hydrostatic stress (pressure) has an important influence on the non-linear behavior of unidirectional composites [28,29]. Voyiadjis and Thiagarajan [30] have proposed a pressure-dependent yield surface for transversely isotropic materials. The invariant-based flow rule and the pressure-dependent transverse isotropic yield function are used in this paper to model the non-linear behavior of the Ciba-Geigy XAS/9l4 unidirectional carbon-fibre/epoxy composite subjected to the 10° off-axis and Iosipescu tests.

2.1. Yield function

A general form of a yield function may be expressed as:

$$\Phi = \phi(\sigma_{ij}) - \phi' \tag{1}$$

where $\phi(\sigma_{ij})$ is the current yield surface and ϕ' is the largest recorded value of $\phi(\sigma_{ij})$ and for initial yield is taken as unity. Voyiadjis and Thiagarajan [30] proposed a pressure-dependent yield function for transverse isotropic materials assuming the behavior in axial tension is the same as in axial compression:

$$\begin{aligned}\phi(\sigma_{ij}) = {} & \frac{2}{9}k_1^2\sigma_{11}^2 + \frac{2}{9}k_2^2(\sigma_{22}^2 + \sigma_{33}^2) \\ & - \frac{2}{9}k_1k_2\sigma_{11}(\sigma_{22} + \sigma_{33}) - \frac{2}{9}k_2^2\sigma_{22}\sigma_{33} + \frac{2}{3} \\ & \times (k_1k_2 + k_4^2)(\sigma_{12}^2 + \sigma_{13}^2) + \frac{2}{3}(k_2^2 + k_6^2)\sigma_{23}^2\end{aligned} \tag{2}$$

where σ_{ij} are stress components in the material coordinate system (aligned with the principal axes of orthotropy) and k_1, k_2, k_4, and k_6 are constants which

describe the yield behavior along various axes. The x_1 axis is assumed to be rotationally symmetric and is therefore parallel to the fiber direction in a unidirectional composite. If a state of plane stress is assumed to exist ($\sigma_{33} = \sigma_{13} = \sigma_{23} = 0$) then Eq. (2) becomes:

$$\phi(\sigma_{ij}) = \frac{2}{9}k_1^2\sigma_{11}^2 + \frac{2}{9}k_2^2\sigma_{22}^2 - \frac{2}{9}k_1k_2\sigma_{11}\sigma_{22} + \frac{2}{3} \times (k_1k_2 + k_4^2)\sigma_{12}^2 \tag{3}$$

The material behavior for any stress state is defined by:

$\Phi < 0$	elastic
$\Phi = 0$	the stress state is on the yield surface, plastic deformation occurring as loading progress
$\Phi > 0$	inaccessible state

If σ_{ij}^{y} represents the initial yield stresses along different directions, then Eq. (3) can be used to obtain expressions of the parameters k_1, k_2, and k_4. In terms of the yield stresses they are:

$$k_1 = \frac{3\sqrt{2}}{2\sigma_{11}^{y}} \quad k_2 = \frac{3\sqrt{2}}{2\sigma_{22}^{y}} \quad k_4 = \sqrt{\frac{3}{2}\left(\frac{1}{\sigma_{12}^{y2}} - \frac{3}{\sigma_{11}^{y}\sigma_{22}^{y}}\right)} \tag{4}$$

For unidirectional carbon-fibre/epoxy composite materials with a fiber-volume fraction of 0.5–0.6, the yield stresses (the start of non-linear behavior in the case of transverse tension and shear) can be assumed to be: $\sigma_{11}^{y} = 1300$ MPa, $\sigma_{22}^{y} = 2$ MPa, and $\sigma_{12}^{y} = 1$ MPa. These yield stresses were used for the purpose of the analysis performed in this study. This assumes that there is no material plasticity along the fibers and the plastic deformation in transverse tension and shear occurs at very low loads. Such assumptions are certainly reasonable considering experimental observations in this research. From Eq. (4), the values of k are: $k_1 = 0.002$, $k_2 = 1.061$, and $k_4 = 1.224$. The form of the yield function indicates that proportional hardening is assumed for this material.

2.2. Flow rule

Hansen et al. [27] have shown that the relationship between the stresses and plastic strains in unidirectional composite materials can be given through the following flow rule [31]:

$$d\varepsilon_{ij}^{p} = g(\sigma_{ij})\left(\frac{\partial\Phi}{\partial\sigma_{rs}}d\sigma_{rs}\right)\frac{\partial\Phi}{\partial\sigma_{ij}} \tag{5}$$

where $d\varepsilon_{ij}^{p}$ is the plastic strain increment tensor and $g(\sigma_{ij})$ is the scalar hardening parameter. Plastic flow occurs when:

$$\frac{\partial\Phi(\sigma_{ij})}{\partial\sigma_{rs}}d\sigma_{rs} > 0 \text{ and } \Phi(\sigma_{ij}) = 0 \tag{6}$$

The scalar hardening parameter, $g(\sigma_{ij})$, is a scalar function of a second-order tensor. It has been shown [27] that $g(\sigma_{ij})$ can be put into a form in which its value depends on the location of the stress state on the yield surface, and is invariant with respect to the material symmetry of the composite. Spencer [32] has shown that the five stress invariants with respect to arbitrary rotations about the axis of symmetry in a transverse isotropic material are:

$$a_1 = \sigma_{11}\, a_2 = \sigma_{\alpha\alpha}\, a_3 = \sigma_{1\alpha}\sigma_{\alpha1}\, a_4 = \sigma_{\alpha\beta}\sigma_{\alpha\beta}$$
$$a_5 = \sigma_{1\alpha}\sigma_{\alpha\beta}\sigma_{\beta1} \quad \alpha, \beta = 2, 3 \tag{7}$$

$g(\sigma_{ij})$ may be therefore put in the form:

$$g(\sigma_{ij}) = g(a_1, a_2, a_3, a_4, a_5) \tag{8}$$

If we assume that the material behaves the same in tension and compression, then we must use quadratic forms of a_1, a_2, and a_5. However, the square of the second invariant is the same as the third invariant under plane stress conditions, so we can disregard a_2. For simplicity, we can also disregard the fifth invariant since it will contain a sixth-order term. It is generally assumed that there is no plastic deformation along the axis of the fibers, therefore a_1 may also be disregarded. Now the scalar hardening parameter is:

$$g(\sigma_{ij}) = g(a_3, a_4) \tag{9}$$

A general form of the scalar hardening parameter may be defined as [27]:

$$g(\sigma_{ij}) = \sum_n \frac{a_n}{a_n^*} g_n(a_n) \tag{10}$$

where the superscript * indicates values of the invariants at the current yield surface assuming a uniaxial invariant stress state. Using Eqs. (9) and (10), the form of the scalar hardening parameter is:

$$g(a_3, a_4) = \frac{a_3}{a_3^*} g_3(a_3) + \frac{a_4}{a_4^*} g_4(a_4) \tag{11}$$

where and $g_3(a_3)$ and $g_4(a_4)$ are functions of each individual invariant and are determined by experiment.

2.3. Experimental characterization

In the off-axis tensile test, the applied tensile load is along the long axis of the specimen, which is defined as the x direction (σ_{xx}) and the fibers are aligned at an angle θ from the loading axis (Fig. 5). A three-element strain gage rosette is mounted at the center of the specimen with one gage aligned along the loading axis, another aligned 45° away from the first, and the third aligned 90° from the loading axis. The material normal and shear stresses (σ_{11}, σ_{22}, and σ_{12}) in the composite may be related to the applied tensile load (σ_{xx}) by:

$$\begin{bmatrix}\sigma_{11}\\ \sigma_{22}\\ \sigma_{12}\end{bmatrix} = \begin{bmatrix}\cos^2(\theta) & \sin^2(\theta) & 2\cos(\theta)\sin(\theta)\\ \sin^2(\theta) & \cos^2(\theta) & -2\cos(\theta)\sin(\theta)\\ -\cos(\theta)\sin(\theta) & \cos(\theta)\sin(\theta) & \cos^2(\theta)-\sin(\theta)\end{bmatrix} \times \begin{bmatrix}\sigma_{xx}\\ \sigma_{yy}\\ \sigma_{xy}\end{bmatrix} \tag{12}$$

Similarly, the total strain components in the material coordinate system may be related to the strain gage strains by transforming the coordinates:

$$\begin{bmatrix}\varepsilon^{t}_{11}\\ \varepsilon^{t}_{22}\\ \varepsilon^{t}_{12}\end{bmatrix} = \begin{bmatrix}\cos^2(\theta) & \sin^2(\theta) & 2\cos(\theta)\sin(\theta)\\ \sin^2(\theta) & \cos^2(\theta) & -2\cos(\theta)\sin(\theta)\\ -\cos(\theta)\sin(\theta) & \cos(\theta)\sin(\theta) & \cos^2(\theta)-\sin^2(\theta)\end{bmatrix} \times \begin{bmatrix}\varepsilon^{t}_{xx}\\ \varepsilon^{t}_{yy}\\ \varepsilon^{t}_{xy}\end{bmatrix} \tag{13}$$

where ε^{t}_{xx} is the strain in the gage aligned along the loading axis $\left(\varepsilon^{t}_{xx}=\varepsilon^{t}_{0^\circ}\right)$, ε^{t}_{yy} is the strain in the gage aligned transverse to the loading axis $\left(\varepsilon^{t}_{yy}=\varepsilon^{t}_{90^\circ}\right)$, and ε^{t}_{xy} is:

$$\varepsilon^{t}_{xy} = \varepsilon^{t}_{45^\circ} - \frac{1}{2}\left(\varepsilon^{t}_{0^\circ}+\varepsilon^{t}_{90^\circ}\right) \tag{14}$$

The experimental plastic strains can be calculated by subtracting the elastic strains from the total strains. The elastic strain components may be calculated as a function of stress components:

$$\begin{bmatrix}\varepsilon^{e}_{11}\\ \varepsilon^{e}_{22}\\ \varepsilon^{e}_{12}\end{bmatrix} = \begin{bmatrix}S_{11} & S_{12} & 0\\ S_{12} & S_{22} & 0\\ 0 & 0 & \frac{1}{2}S_{66}\end{bmatrix}\begin{bmatrix}\sigma_{11}\\ \sigma_{22}\\ \sigma_{12}\end{bmatrix} \tag{15}$$

where

$$S_{11}=\frac{1}{E_1}\,S_{12}=-\frac{\nu_{12}}{E_1}=-\frac{\nu_{21}}{E_2}\,S_{22}=\frac{1}{E_2}\,S_{66}=\frac{1}{G_{12}} \tag{16}$$

where E_1, E_2 are the axial moduli parallel and transverse to the fibers, respectively. G_{12} is the longitudinal shear modulus, and ν_{12} and ν_{21} are Poison's ratios. The elastic properties of the composite were experimentally determined from 0°, 10° and 90° off-axis tensile tests and were found to be:

$E_1 = 140$ GPa
$E_2 = 11$ GPa
$G_{12} = 6$ GPa
$\nu_{12} = 0.38$

The scalar hardening parameter for a particular material can be determined from two off-axis tests. The parameter $g_3(a_3)$ can be determined using Eq. (5) and the plastic strains obtained from a 90° off-axis test [in this case $g_3(a_3) = g(a_3, a_4)$]. An arbitrary off-axis angle may then be used to determine $g_4(a_4)$ by again using Eq. (5) and experimental data to obtain $g(a_3, a_4)$. Thus, from the experimentally determined $g_3(a_3)$ and $g_4(a_3)$, $g(a_3, a_4)$ may be calculated for any plane-stress state of any unidirectional composite material.

3. Experimental procedure

3.1. Iosipescu shear test

0° Iosipescu specimens of Ciba-Geigy XAS-914 unidirectional carbon-fibre/epoxy composite material were machined to the dimensions suggested by the ASTM standard. Two three-element rosette strain gages (Measurements Group WK-06-060WR-350) were mounted in the center of the specimens (one on each side) in order to measure the total strain in the middle of the notch-root axis. A biaxial Iosipescu test fixture was used [11,33] with loading blocks that are the same dimensions as that suggested by the ASTM standard. The tests were performed on a servo-hydraulic MTS 880 with hydraulic grips and a displacement rate of 0.5 mm/min. Load and strain data were taken up to a fixture displacement of about 2.5 mm. The shear strain was calculated from the strain-gage reading by the relationship:

$$\gamma_{12} = \varepsilon_1 - \varepsilon_2 \tag{17}$$

where ε_1 and ε_2 are the strains measured by the strain gage elements that are ±45° to the principal material coordinates (see Fig. 1). The strains from the gages on both sides of the specimen were averaged. The shear stress was determined by taking the load as read by the load cell and dividing by the cross-sectional area of the gage section of the specimen.

3.2. Off-axis tensile tests

The 10° and 90° off-axis test specimens were machined to dimensions similar to those recommended by ASTM D3039-76. The 10° off-axis specimens were 200 mm long, 12 mm wide, with an as-received thickness of 5 mm. The 90° specimens were 120 mm long, 25 mm wide, and 5 mm thick. Three-element rosette strain gages were mounted in the center of the specimen aligned as described above. Aluminum tabs were used at the gripped portions of the specimen to prevent specimen crushing by the serrated (diamond-faceted) grip faces. The grips for the 90° specimen were straight and those for the 10° specimen had an oblique angle of 22°. The tabs were bonded to the specimen with an epoxy adhesive. The tests were performed on the same testing machine as that used for the Iosipescu specimens. All of the specimens failed in the gage section away from the gripped areas.

In the 10° off-axis test, the shear stress and shear strain (in the material coordinate system) are calculated by transforming the applied stresses and measured strains (from the strain gages) using Eqs. (12) and (13). The stress and strain data required to determine the elastic-plastic properties of the carbon-fibre/epoxy composite were obtained from two 10° and two 90° off-axis tensile tests. The values of the components of the scalar hardening parameter were determined to be (using the procedure described above):

$$g_3(a_3) = \left(2.0 \times 10^{-11}\right)a_3$$
$$g_4(a_4) = \left(1.25 \times 10^{-8}\right)a_4 \tag{18}$$

Therefore, the scalar hardening parameter is:

$$g(\sigma_{ij}) = \left(2.0 \times 10^{-11}\right)\sigma_{12}^2 + \left(1.25 \times 10^{-8}\right)\sigma_{22}^2 \tag{19}$$

This parameter was determined by using stress in units of MPa and dimensionless tensorial strains.

4. Finite-element models

Three non-linear finite-element models (10° off-axis, Iosipescu with no axial splits at the notches, and Iosipescu with two axial notch-root splits) were created in order to examine the stresses and strains in the specimens. All three models assumed geometric non-linearity and material non-linearity. The Iosipescu models also assumed boundary contact non-linearity between the specimen and loading blocks. The resulting numerical stress/strain data can be directly compared to the experimental results in order to determine if the plasticity model outlined in Section 2 can accurately describe the composite behavior. Then, stresses and strains in the specimens may be calculated and used to determine the actual shear strength.

4.1. Iosipescu models

Two finite-element models of the Iosipescu shear test (with and without notch-root axial splits) simulated the loading conditions of the modified Wyoming fixture. The computations were performed with ANSYS® 5.4. The models are two-dimensional (having a thickness of unity, i.e. 1 mm) and use isoparametric elements with eight nodes (PLANE82). Point-to-surface contact elements (CONTAC48) were used to simulate sliding between the loading blocks and the composite specimen with a friction coefficient of $\mu = 0.3$. This friction coefficient was chosen based on an expected value of a static friction coefficient between steel loading blocks and an unidirectional carbon-fibre-reinforced polymer composite. It has been previously shown that the effect of the friction coefficient on the numerical load/strain and load/displacement curves is negligible for unidirectional composite Iosipescu specimens within the range of 0.1–0.5 [15,16]. For the model with the notch-root splits, the length of the cracks was 9 mm, which was chosen based on the average split length observed experimentally for this particular composite.

The mesh and boundary conditions used in the analysis are shown (Figs. 6 and 7) with a deformed finite-element representation of the specimen. The specimen center was constrained against vertical and horizontal displacements (u_x and $u_y = 0$). The blocks on the right side of the specimen had prescribed displacements of $u/2$ and the blocks on the opposite side were loaded by a negative displacement of the same magnitude. Thus, the total prescribed displacement acting on the specimen was equal to u. The total reactions from each node on the right loading blocks were summed (this is equal to the load as read by a load cell in the experiment). Also, all stress and strain components were calculated along the notch-root axis of the specimens using the nodal displacements (including the strains in the middle for modeling the three-element rosette strain gage).

The loading procedure for both models was divided into a minimum of 40 load steps. Each load step had a maximum of 25 equilibrium iterations, and during each iteration the square root of the sum of squares (SSRS) of the imbalance forces were calculated. The force convergence criterion was assumed with the SRSS of the imbalance forces smaller than 0.1% of the SRSS of the loading forces.

4.2. 10° off-axis model

The model of the 10° off-axis tensile test is three-dimensional and uses isoparametric 10 node tetrahedral

elements (SOLID92) (see Fig. 8). The 10° off-axis specimen has one plane of symmetry in the plane of the thickness ($z = 0$). The gripping tab is modeled as aluminum, oblique, and perfectly bonded to the composite specimen. These assumptions are consistent with the experiment.

The boundary conditions used in the analysis are shown in Fig. 8. The back face of the specimen is constrained against displacements in the z-direction at each node in order to satisfy the conditions of a plane of symmetry. Each node on the front face of the top tab is displaced in the direction of the loading axis by $u/2$. The bottom tab has a negative displacement with an equal magnitude. Thus, the total prescribed displacement acting on the specimen is equal to u. The total reactions from each node on the top tab were summed and doubled (on account of the plane of symmetry), which is equal to the load as read by a load cell in the

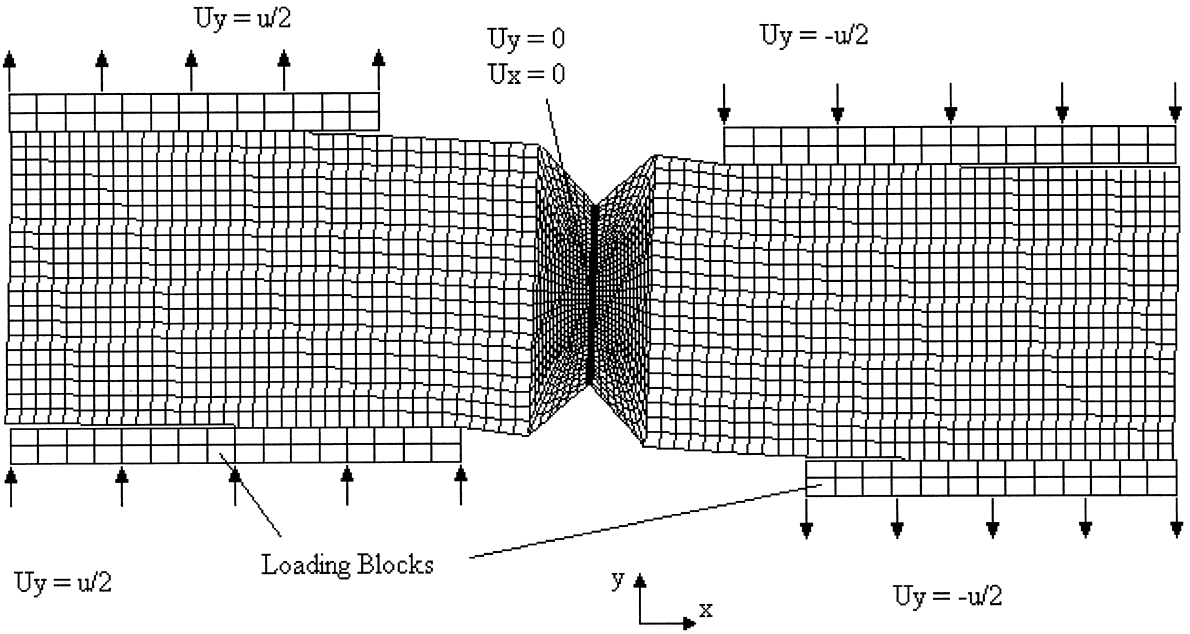

Fig. 6. The finite element model of the Iosipescu specimen without axial splits. The element mesh, boundary conditions, global coordinate system, and loading blocks are shown.

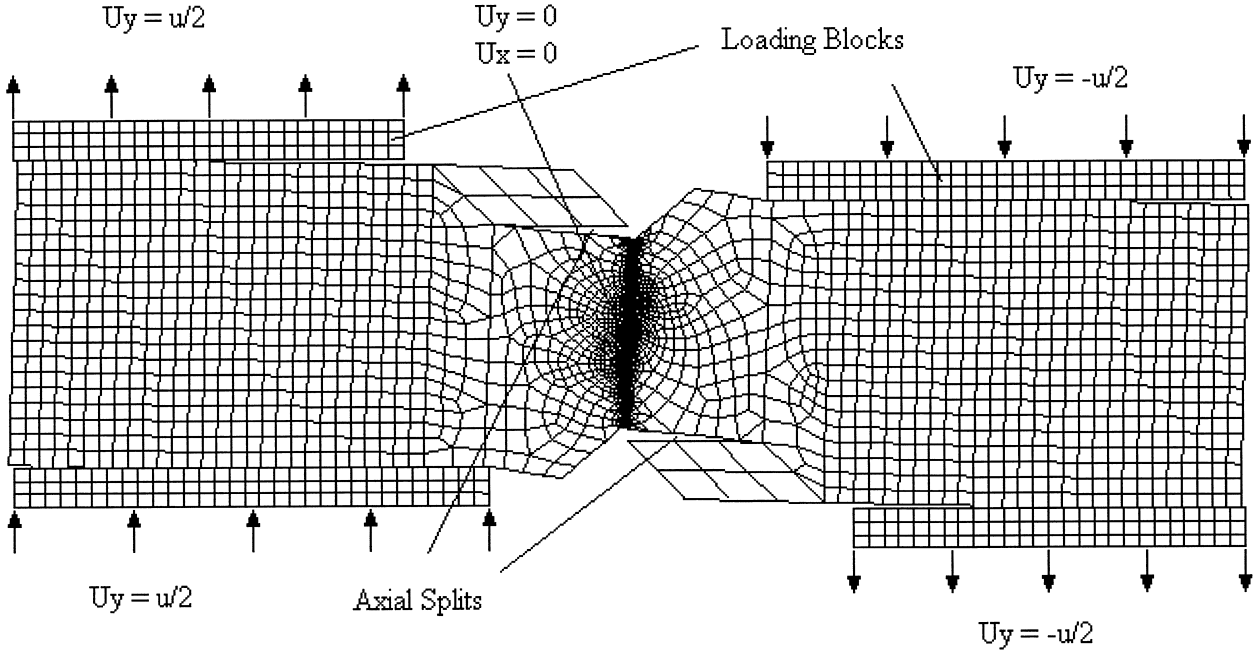

Fig. 7. The finite-element model of the Iosipescu specimen with axial splits. The element mesh, boundary conditions, and loading blocks are shown.

experiment. A numerical strain gage was added at the center of the specimen to model a three-element rosette strain gage. The strains were calculated from the displacements at each node in the gage and averaged. The loading procedure is the same as that for the Iosipescu model.

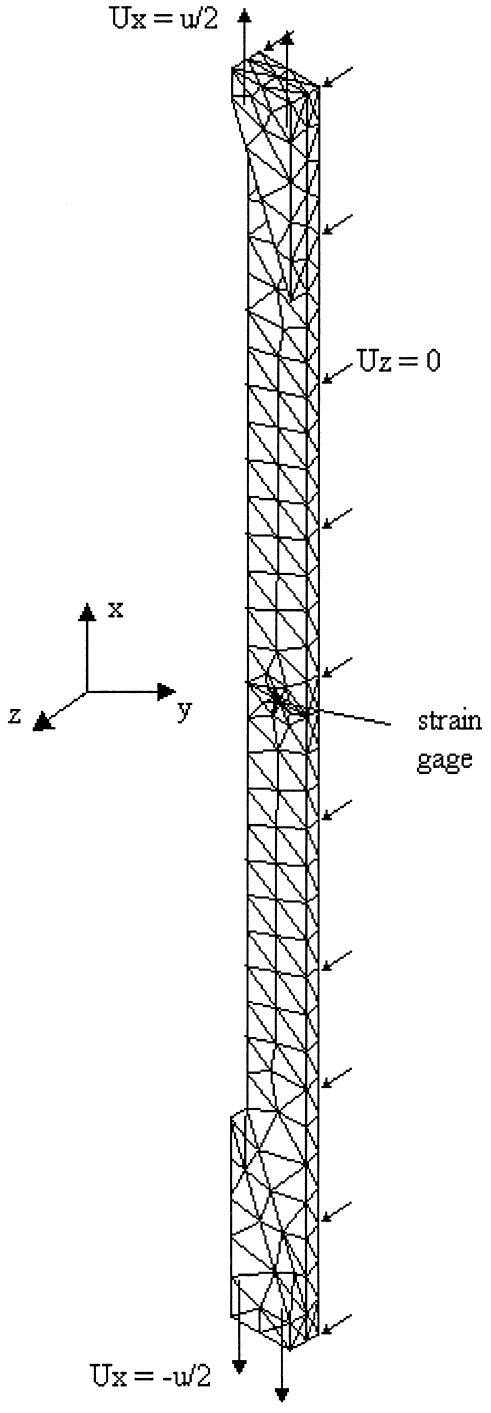

Fig. 8. The finite-element model of the 10° off-axis test with element mesh, boundary conditions, global coordinate system, numerical strain gage, and oblique tabs shown.

4.3. Modeling material non-linearity

Because of the computational tools currently available to this research (ANSYS® 5.4) there is a critical limitation to the way elastic/plastic properties of anisotropic materials can be modeled. The non-linear stress/strain curve for a composite material must be estimated with a bi-linear approximation. The slope of the first line is the elastic portion, and the slope of the second line is the plastic portion. The point were the two linear curves intersect is defined as the yield strength. This estimate must be input for the separate cases of pure axial stress along the three principal axes of the fabric composite, i.e. along each fiber direction and through the thickness of the specimen. Also, this must be input for the three cases of pure shear. Clearly, this is not strictly accurate for modeling the elastic/plastic behavior of either unidirectional or fabric composite materials since there is no sharp cut-off between the elastic and plastic portions of the stress/strain curve and the plastic stress-strain behavior of composites is not linear but follows a non-linear-type hardening curve. A method has been recently developed to overcome this difficulty [34]. The elastic/plastic stress/strain response of the unidirectional composite material was approximated with a multi-linear fit as input into the finite-element code. The stress/strain response estimated with the plasticity model in Section 2 was calculated for the cases of pure shear and pure transverse tension and a series of bi-linear fits were fitted to this curve, then averaged to produce a multi-linear fit that estimated the response very closely up to a desired strain. The finite-element model was solved for each bi-linear fit and the resulting load, stress, and strain values were averaged.

For the numerical models the multi-linear fits were approximated with four bi-linear curves. This was done by taking four points along the stress/strain curves for pure shear and transverse tension and optimizing the four curves so that their average at these points was the same as the value of the curve at that point. This insured that the value of the average line closely followed the response curve line between these four points. At the first approximation point one of the bi-linear lines changed its slope while the others maintained their original slope. At the next point, another bilinear line changed its slope, and the second slope of the line that changed its slope at the first approximation point was changed so that the average of all of the bi-linear fits was the same as the value at the second approximation point. For each successive point, a bi-linear fit changes to its second slope, and the second slope of the bi-linear fit that changed its slope in the previous point is adjusted to maintain the average so that it is equal to the response curve at that approximation point. Thus, with four approximation points there are four bi-linear fits

and five total slopes to with which estimate the stress/strain responses. Each bi-linear fit assumed a different value of the elastic shear and transverse moduli. Occasionally, it is impossible to maintain the average at each point, and the process must start over with different original slopes before the first approximation point for each bi-linear fit. Figs. 9 and 10 show the stress/strain response curve in pure shear and transverse tension with the bi-linear approximations and the average curve.

This procedure was repeated for the case of larger strains (as experienced by the Iosipescu specimen at a 2-mm fixture displacement). The material response curves in pure shear with bilinear approximations for this case are shown in Figs. 11 and 12.

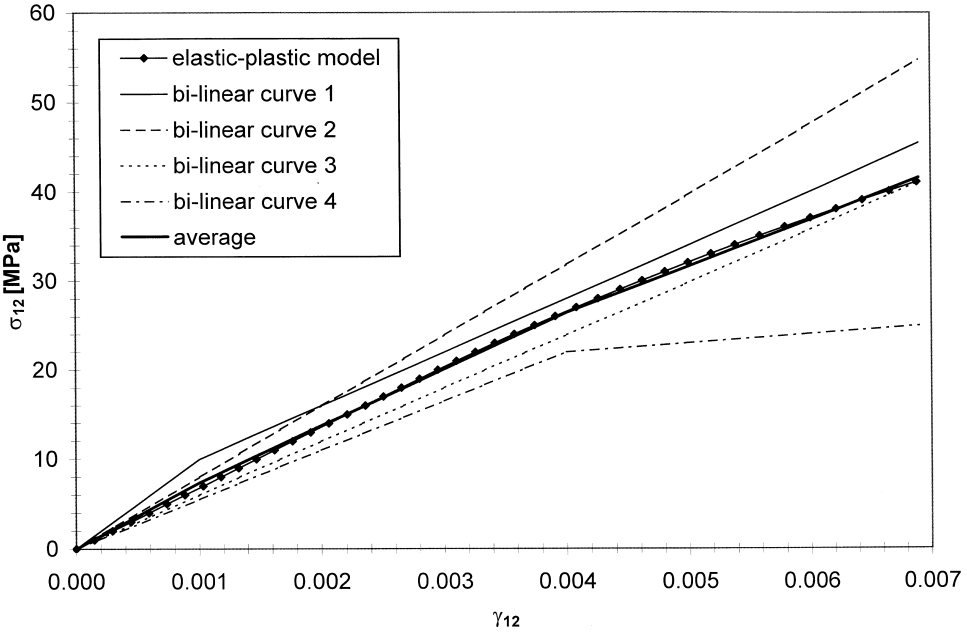

Fig. 9. Shear-stress/total-strain diagram (for small strains) of the elastic/plastic response of the material with four bilinear approximations and average multi-linear curve.

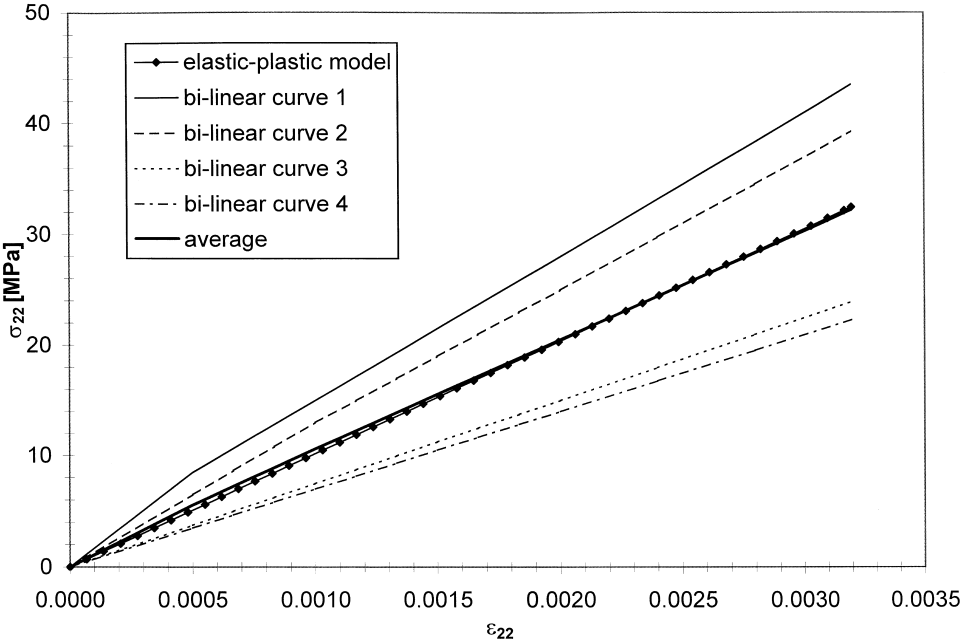

Fig. 10. Transverse-stress/total-strain diagram (for small strains) of the elastic/plastic response of the material with four bilinear approximations and average multi-linear curve.

5. Results and discussion

5.1. Shear stress/strain diagrams of the 10° off-axis and Iosipescu tests

5.1.1. 10° off-axis test

The numerical and experimental tensile stress/strain curves (loaded along the x axis) for the 10° off-axis test are presented in Fig. 13. The elastic/plastic curve matches the experiments very closely which indicates that the non-linear finite-element model describes the behavior of the composite in the 10° off-axis experiment very accurately. The elastic/plastic curve is between the two experimentally obtained plots. The stress/strain curve from the linear/elastic model slightly overestimates the mechanical response of the composite in comparison

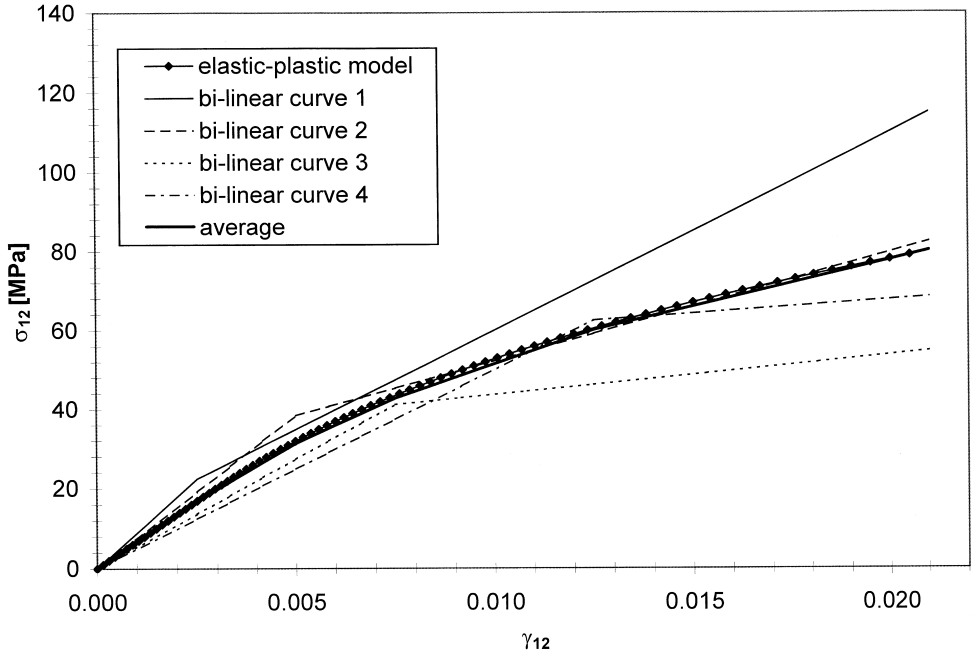

Fig. 11. Shear-stress/total-strain diagram (for large strains) of the elastic/plastic response of the material with four bilinear approximations and average multi-linear curve.

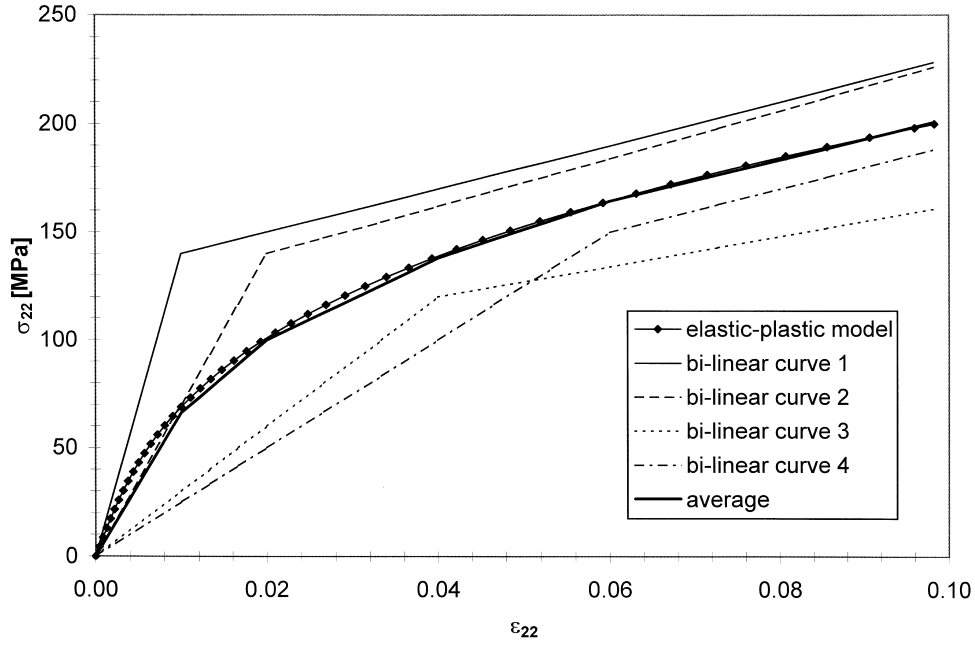

Fig. 12. Transverse-stress/total-strain diagram (for large strains) of the elastic/plastic response of the material with four bilinear approximations and average multi-linear curve.

with the two experimental and the numerical elastic/plastic curves.

5.1.2. Iosipescu test

Fig. 14 shows the numerical and experimental shear stress/strain curves for the Iosipescu shear test. The experimental curve contains characteristic load drops as a result of the two axial notch-root splits that form during the test. The overall shape of the experimental shear stress/strain curve does not change significantly from test to test, however, the location of the load drops resulting from the notch-root splitting vary significantly. Clearly, the linear/elastic model is a very poor estimate of the actual mechanical response of the specimen when subjected to shear (except in the small strain region). The numerical elastic/plastic model without splits follows the experiment very closely until the first split occurs. The model with splits initially follows the experiment after the second split. Between the splits the value of the experimentally determined shear stress

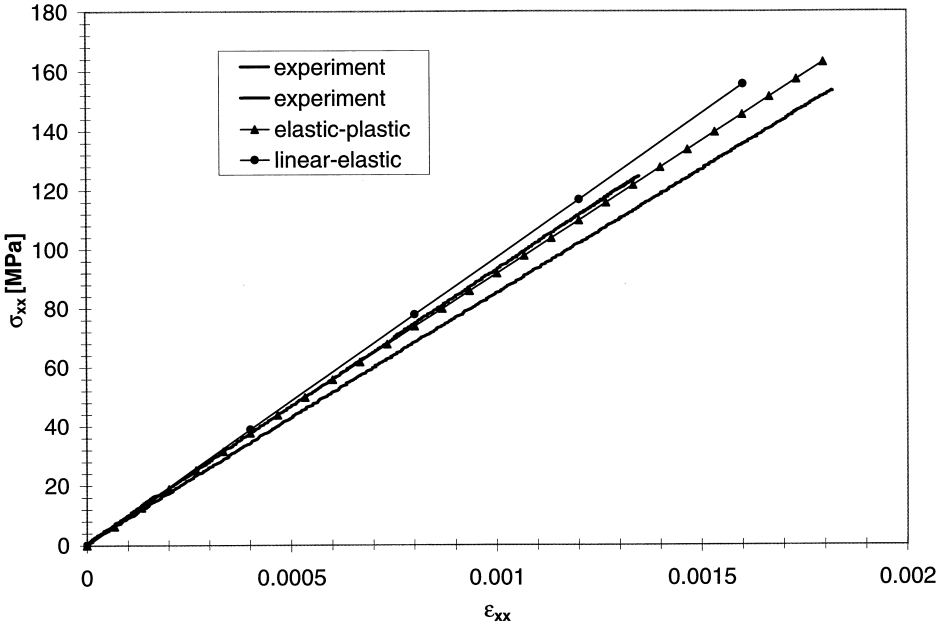

Fig. 13. Numerical and experimental axial stress/strain curves for the 10° off-axis test. The stress is calculated from the fixture load divided by the specimen cross-sectional area. The shear strains are calculated from strain gages mounted in the test section.

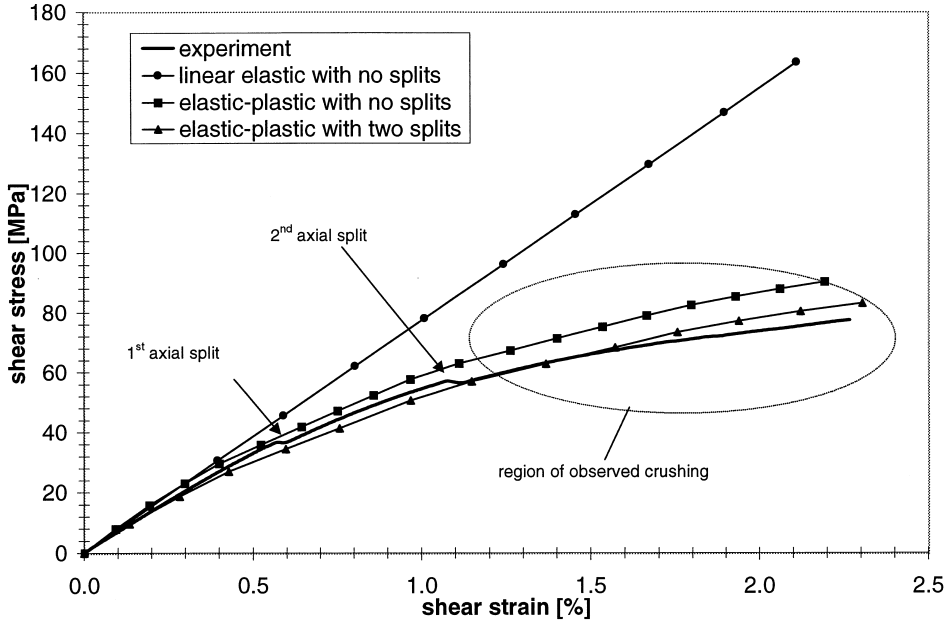

Fig. 14. Numerical and experimental shear stress/strain curves for the Iosipescu shear test. The shear stress is calculated from the fixture load divided by the specimen cross-sectional area. The shear strains are calculated from strain gages mounted in the test section.

(P/A) is between the values of the shear stresses from the models with and without the notch-root splits. However, it can be observed that the numerical non-linear two split model diverges from the experiment at higher shear strains. This is a result of the crushing of the specimen in areas directly adjacent to the loading blocks (mode 4 in Fig. 2). The plastic deformation of the material in the vicinity of the loading blocks was simulated by the non-linear finite-element models.

However, the crush zones consist of numerous interlaminar and intralaminar cracks. The formation of these cracks was not considered in the finite-element analyses. Therefore, the numerical curve diverges from the experimental response because of the development of crush damage zones near the loading blocks which the present non-linear model cannot accurately handle. Moreover, failure modes 2 and 3 (in Fig. 2) will also affect the divergence of the numerical and experimental curves. Since crushing and intralaminar failure cause a greater load reduction than the material non-linearity (that is modeled by using the plasticity theory given above), the numerical model over-predicts the experiment when crushing becomes significant. Adams and Lewis [35] have shown that crushing may become significant after the second notch-root split occurs in certain unidirectional composites, which reinforces the data presented here. However, crushing can also occur at lower loads, even as low as those associated with notch-root splitting [16]. Therefore, the location of the point where the numerical two-split model diverges from the experiment can vary from specimen to specimen even for the same material.

5.2. Effect of element size near the notch-root

In order to properly determine the internal stresses and strains near the roots of the notches and explain the failure process in the Iosipescu specimen under non-linear conditions, it is necessary to understand the effect of the element size on the calculations of the local stress and strain fields in these areas. Therefore, a study of the effect of element size on numerical stress calculations using the fully non-linear Iosipescu model without notch-root splitting has been performed.

The size of the elements near the notch-root was varied in the finite-element model of the Iosipescu specimen. The stresses and strains were calculated along the notch-root axis near the tip of the notch-root for each element size and compared. Figs. 15–20 show plots of these stress and strain components. Clearly, there is a significant change in the calculations depending upon the element size. For all of the stress and strain components, there appears to be an asymptotic value near the notch-root that is approached as the element size is decreased. More importantly, the maximum value of the shear stress and shear strain changes not only in magnitude but in location. As the element size is decreased, the maximum increases and the location shifts closer to a point near the notch-root. The choice of element size should be based on accuracy and efficiency. There appears to be a negligible difference in the calculations of the magnitude and location of the maximum shear stress and shear strain between the 0.067 and 0.075 mm element sizes. The difference in the normal components of stress and strain between these element sizes is also negligible. However, when the element size is reduced

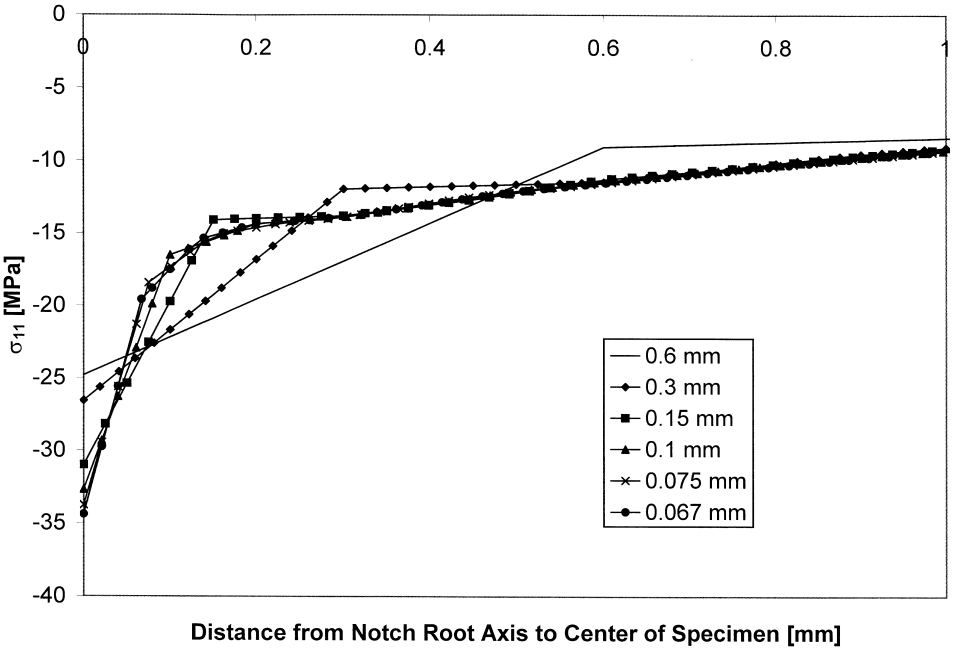

Fig. 15. Normal stress (parallel to fibers) plotted along the notch-root axis for various element sizes.

below 0.075 mm, the error becomes more significant, especially in the calculation of the location of the maximum shear stress and strain. Therefore, a compromise between accuracy and time efficiency favors the use of the element with a side length of 0.075 mm for the unidirectional carbon-fibre/epoxy Iosipescu specimens modeled in this research. However, the critical element size can be strongly dependent on the non-linear material properties of unidirectional composites. This effect has not been investigated in this study.

5.3. Stresses in 10° off-axis and Iosipescu specimens

In this section, the stress distributions in the 10° off-axis and 0° Iosipescu specimens were compared in order to determine the shear strength of the Ciba-Geigy XAS-914 composite from these two independent tests.

5.3.1. 10° off-axis test

The 10° off-axis specimens used in this study failed at relatively low tensile loads, most likely as a consequence

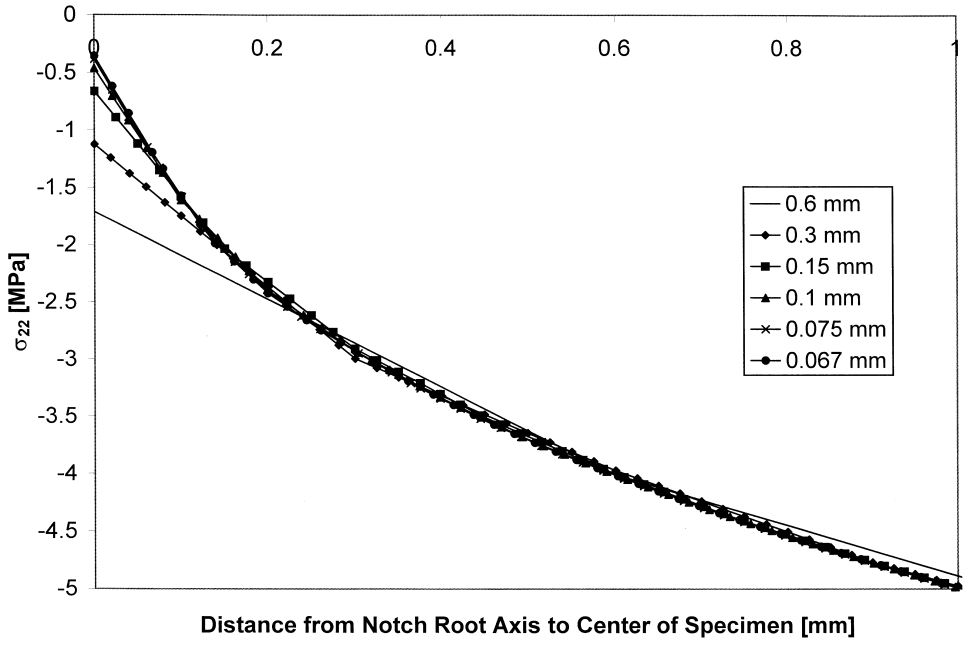

Fig. 16. - Normal stress (perpendicular to fibers) plotted along the notch-root axis for various element sizes.

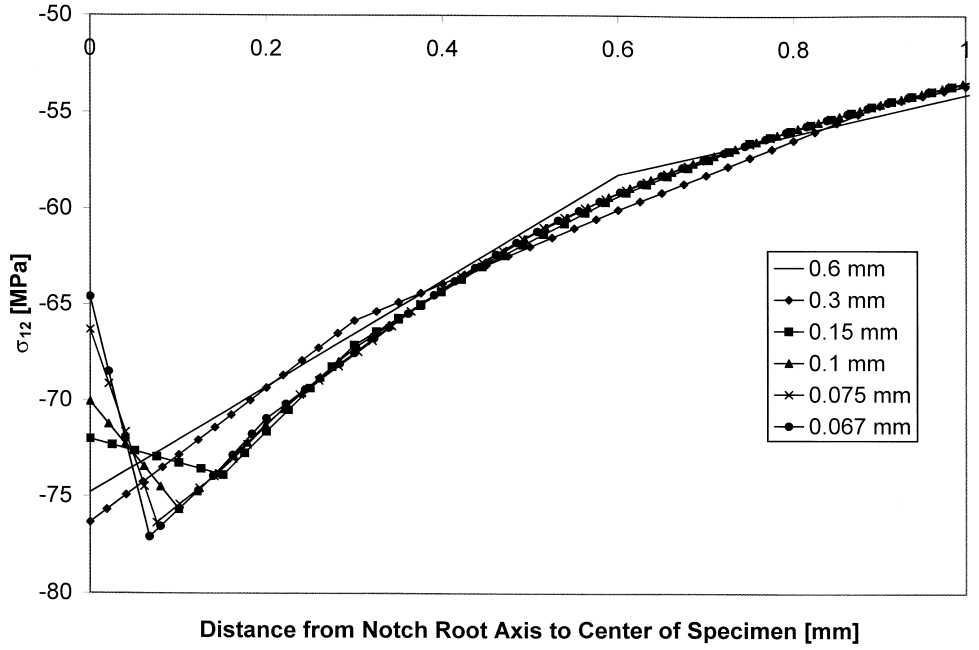

Fig. 17. Shear stress plotted along the notch-root axis for various element sizes.

of inadequate machining. Therefore, for the purposes of determining the actual shear strength of the composite, the data obtained by Balakrishnan et al. [22] will be used in this study. The 10° off-axis test conducted by Balakrishnan et al. [22] were performed on exactly the same carbon-fibre/epoxy Ciba-Geigy XAS-914 composite as used in this research. Out of all the of the 10° off-axis data available in this research and the data already published for this particular composite (nine total 10° off-axis tests), the highest loads at failure were taken in order to minimize the effect of different machining methods and specimen failures close to the grips.

The failure loads of two specimens (that failed in the gage section) with the same dimensions were 25.8 and 28.6 kN from Balakrishnan et al. [22] and the respective shear stresses at failure were found to be 71.6 and 79.4 MPa [using Eq. (12)]. The linear-elastic and non-linear finite element models of the 10° off-axis test (with the same specimen dimensions) were run with iterative displacements until a load of 27 kN was reached which is

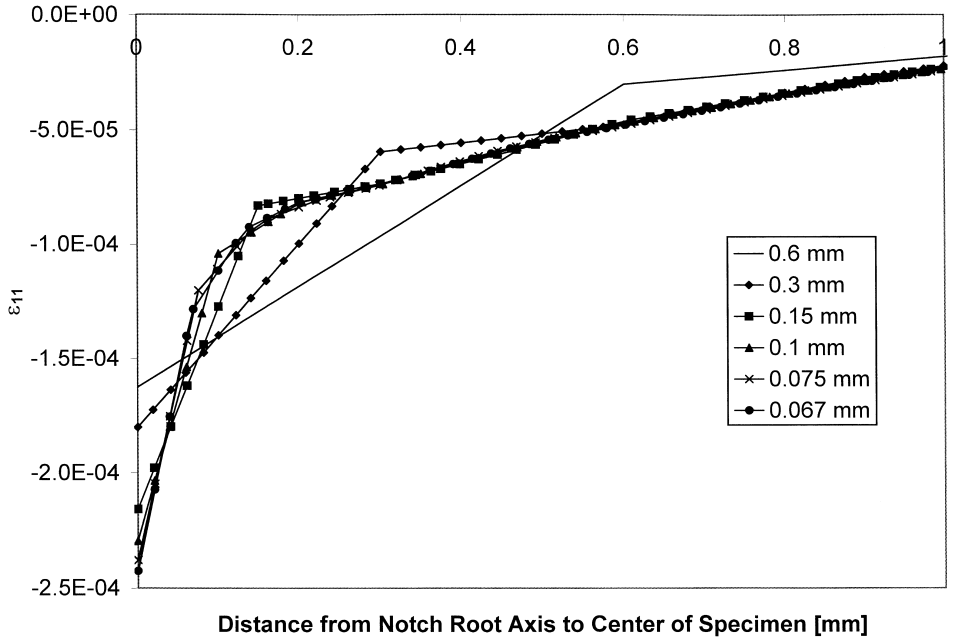

Fig. 18. Normal strains (parallel to fibers) plotted along the notch-root axis for various element sizes.

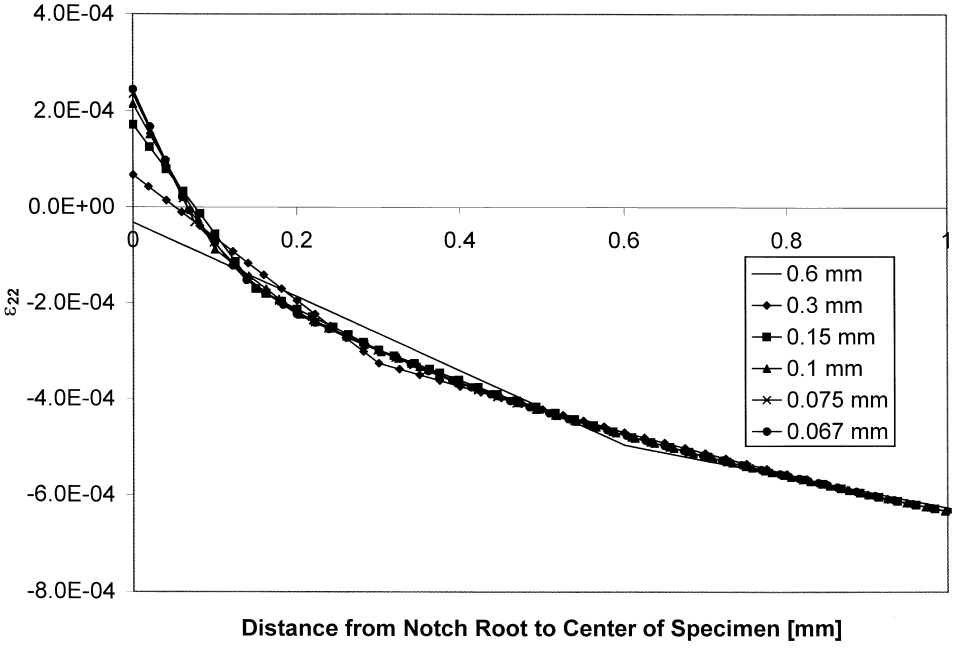

Fig. 19. Normal strains (perpendicular to fibers) plotted along the notch-root axis for various element sizes.

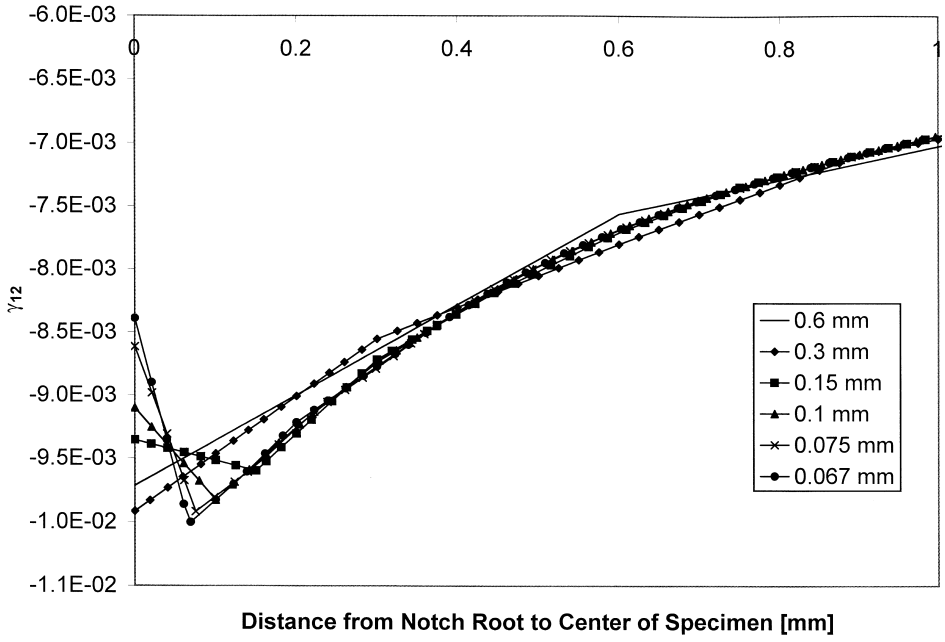

Fig. 20. Shear strains plotted along the notch-root axis for various element sizes.

almost the average load for these two tests. It was determined that the stresses in the specimen did not change significantly throughout the gage section (through the thickness, along the width, and along the length) for a given applied load. The average shear stresses in the linear/elastic and elastic/plastic models were 67.4 and 67.2 MPa, respectively (in the material coordinate system calculated at the nodes). The normal and shear stresses in the specimen gage section obtained from the finite-element model for an applied load of 27 kN are presented in Table 1.

It can be seen that the stresses calculated from Eq. (12) (analytical) and the linear/elastic model of the 10° off-axis test are not the same. In particular, Eq. (12) overestimates the shear stress by approximately 6%. The normal stress σ_{zz} is overestimated by 17%. Most importantly, there is a small effect of material non-linearity on the stresses if the numerically determined stress fields are compared. Since the stress field in the 10° off-axis test is essentially biaxial, a multi-axial failure criterion must be used to extract the actual shear strength of the composite from both the analytical and numerical stresses.

The Tsai–Wu [36] failure criterion was used to extract the shear strength due to the influence of normal stresses by using stress values obtained from the linear/elastic and fully non-linear finite-element models. In addition, the failure criterion was also used to determine the shear strength of the composite analytically from Eq. (12). The strength values used in the failure criterion for carbon-fibre/epoxy were based on data from Balakrishnan et al. [22] for Ciba-Geigy XAS-914 and ASM Committee [37] for carbon-fibre/epoxy composites in general:

$X_t = 1000$ MPa [37]
$X_c = 700$ MPa [37]
$Y_t = 40$ MPa [22]
$Y_c = 120$ MPa [37]

where X and Y are the strengths parallel and transverse to the fibers, respectively, and the subscripts t and c denote tension and compression, respectively. The resulting shear strengths were calculated to be 76.9, 77.0 and 83.6 MPa for the linear/elastic and non-linear finite element models and the analytical model, respectively (also listed in Table 1). As for the stresses, the shear strength of the composite obtained from the 10° off-axis test and using Eq. 12 (analytical model) is overestimated by 8.6% in comparison with the linear/elastic and fully non-linear finite-element models.

5.3.2. Iosipescu test

Figs. 21–23 present the numerically calculated stress components along the notch-root axis for 10 load

Table 1
Stresses in the 10° off-axis test calculated numerically and analytically with the shear strength calculated from the Tsai–Wu failure criteria [36] shown

	Analytical (MPa)	Numerical (MPa)	
		Linear/elastic	Elastic/plastic
σ_{11}	418.5	414.0	392.9
σ_{22}	12.6	10.8	11.8
σ_{12}	71.5	67.4	67.2
τ_c	83.6	76.9	77.0

sub-steps (up to 1 mm fixture displacements) for the fully non-linear models with and without axial notch-root splits. For the 1 mm displacement sub-step, the corresponding shear stresses determined from the global applied load divided by the specimen cross-sectional area are shown in Fig. 23. For the model with splits, the shear stress determined from the total load is 34.5 MPa whereas for the model without the splits the shear stress was found to be 41.3 MPa. Since the linear/elastic models of the Iosipescu specimens with and without axial splits grossly overestimate the mechanical behavior determined experimentally (see [15]), the stress distributions from the linear/elastic models are not presented nor discussed here.

Fig. 21 shows that the normal stresses along the fibers are relatively uniform in the center of the test section along the notch-root axis for both non-linear models, but have large compressive stress concentrations near the notch-roots. The notch-root splitting increases the magnitude of the compressive σ_{11} stresses near the notches. Fig. 22 shows that the compressive transverse normal stresses (σ_{22}) are relatively uniform in the center

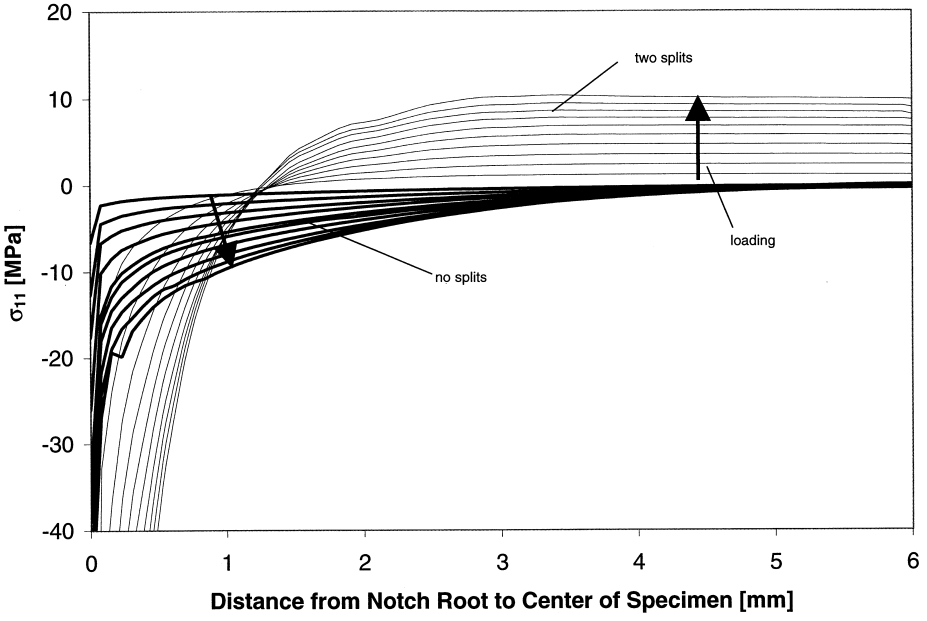

Fig. 21. Normal stress (parallel to fibers) plotted along the notch-root axis over 10 sub-steps for Iosipescu models with and without axial splitting. Progressive loading is indicated.

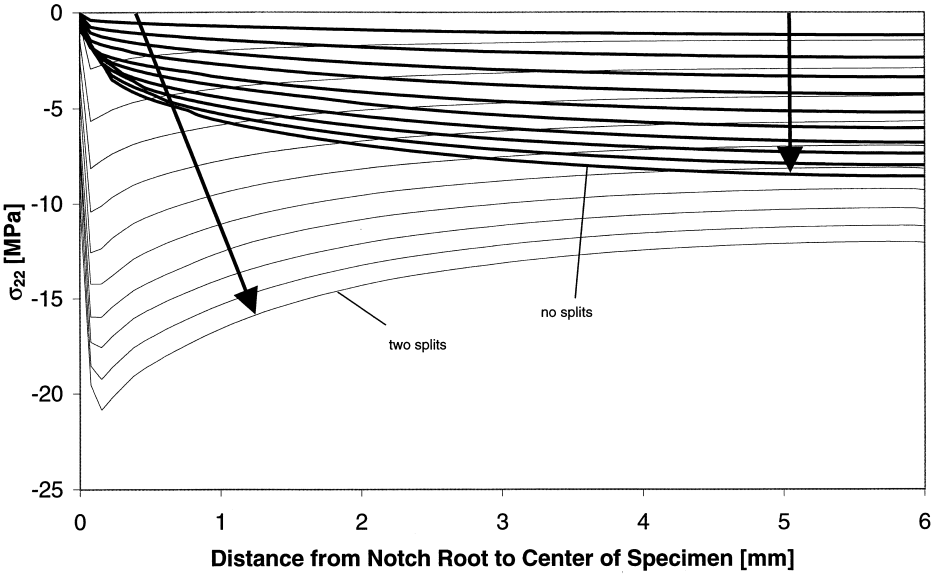

Fig. 22. Normal stress (perpendicular to fibers) plotted along the notch-root axis over 10 sub-steps for Iosipescu models with and without axial splitting. Progressive loading is indicated.

of the specimen with the stresses higher for the model with notch-root splitting. However, the transverse normal stress distributions near the notches are significantly different for the two non-linear models. The splitting causes a rise in the magnitude of the normal transverse compressive stresses near the notches.

It can be seen in Fig. 23 that the shear stresses are very uniform along the notch-root axis after the splitting occurs, with a slight concentration near the notch-root. At a fixture displacement of 1.0 mm, the shear stress in the center of the test section is nearly equal to the shear stress determined from the global load divided by the specimen cross-section (with an error of 3.1%). After axial splitting occurs, the concentrations near the notch-roots are small (about 21% larger than at the center of the specimen). The shear stress concentration in the model without splitting is significantly larger.

In addition to the stresses along the notch-root axis presented in Figs. 21–23, stress distributions in the specimen gage section for the models with and without the

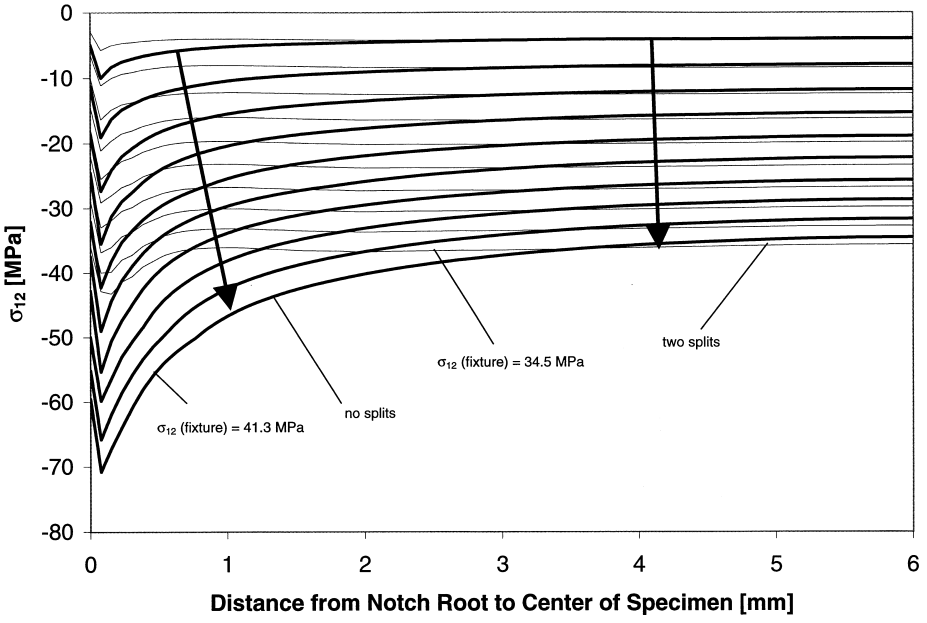

Fig. 23. Shear stress plotted along the notch-root axis over 10 sub-steps for Iosipescu models with and without axial splitting. Progressive loading is indicated.

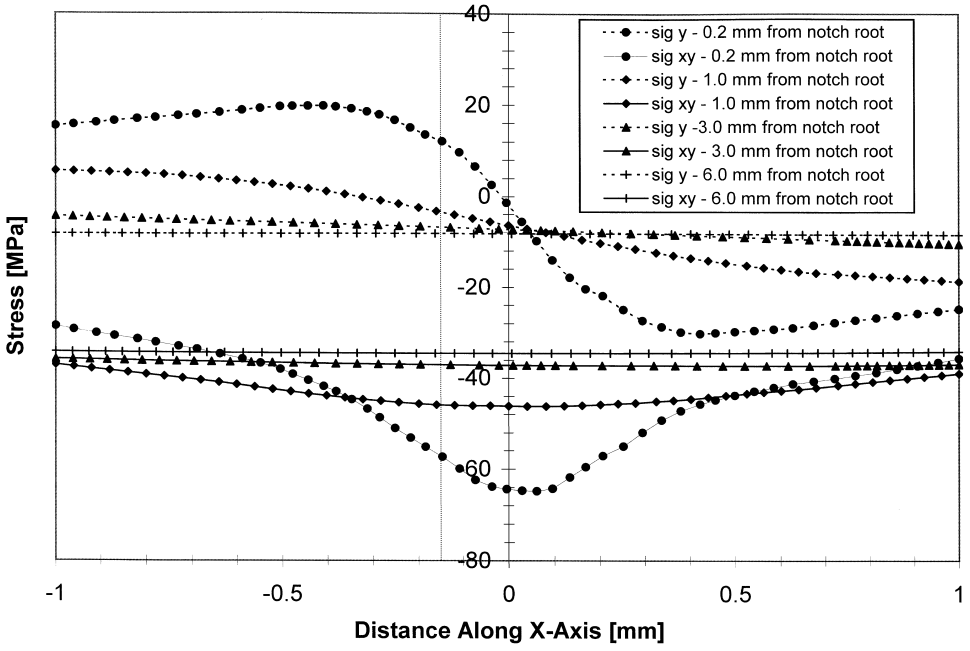

Fig. 24. Stresses parallel to the x axis near the notch-root for the Iosipescu model without notch-root splits.

notch-root axial splits were examined parallel to the x axis of the specimens. The shear (σ_{12}) and transverse normal (σ_{22}) stresses are plotted in Figs. 24 and 25 at distances of 0.2, 1, 3, and 6 mm from the notch-root. It can be seen that these stress components are significantly affected by the presence of notch-root splits. For the specimen without the notch-root splits, the shear-stress distributions are almost symmetric with respect to the notch-root axis, and the transverse normal stresses are not. The stresses on the right side (the side of the inner loading block) are compressive, whereas the stresses on the other side of the specimen are tensile. The tensile stresses very close to the notch-root axis increase as the distance from the notch-root decreases. The stress distributions along the x axis of the specimen with the notch-root splits are significantly different (see Fig. 25). In this case, the normal transverse stresses are always negative on both sides of the notch-root axis with the compression on the side of the inner loading block higher than on the opposite side. The effect of these two completely different stress fields on the specimen failure modes will be discussed in the section below.

5.3.3. Comparison of the tests in terms of stresses

In order to evaluate the shear strength of unidirectional composites by using 0° Iosipescu specimens subjected to shear, the failure modes must be identified and discussed in detail. The most common failure mode is the formation of two axial splits near the roots of the notches along the notch flank (mode 1 failure). The split-formation process is associated with two load drops on the load/displacement curves and is determined by the notch geometry and the local stress concentrations in these areas. In addition, the damage caused by specimen machining can also significantly affect the loads at splitting. These notch-root splits should not be considered as the intralaminar shear-failure process. The second failure mode is the formation of large intralaminar cracks parallel to the x axis of the specimen. Both the notch-root splits (1) and the axial cracks (3) can be easily observed using optical microscopy. However, in some composites, for example in the glass/polyester specimen shown in Fig. 4, the large splits below the roots of the notches have not been observed. In addition to the axial cracks 1 and 3, two continuous intralaminar damage zones (type 2 failure) are formed in the immediate vicinity of the notch-roots consisting of numerous short (microscopic) cracks along the fibers. In transparent glass-fibre/polymer composites type 2 cracks can be easily observed visually. However, in unidirectional carbon-fibre/epoxy composite materials these intralaminar damage zones are not easily detected. In addition to the crack/damage zones 1, 2, and 3, large crush zones (mode 4 failure) may initiate in Iosipescu specimens near the loading blocks at different loads.

In Figs. 3, 4, and 26 examples of the above failure modes are presented. In the case of the glass/polyester specimen (see Fig. 4) the axial splits (1) near the notches as well as the damage zones near the notch-roots (2) and the loading blocks (4) are readily observed. In this particular case the larger intralaminar cracks (3) were not detected. A nice example of a split (1), two axial cracks (3), and a small damage zone (2) can be seen in Fig. 3 for a unidirectional carbon-fibre/PEEK Iosipescu specimen. It can be noticed that the axial cracks in the specimen gage section are opened, especially the first large crack from the notch-root. The small cracks in the

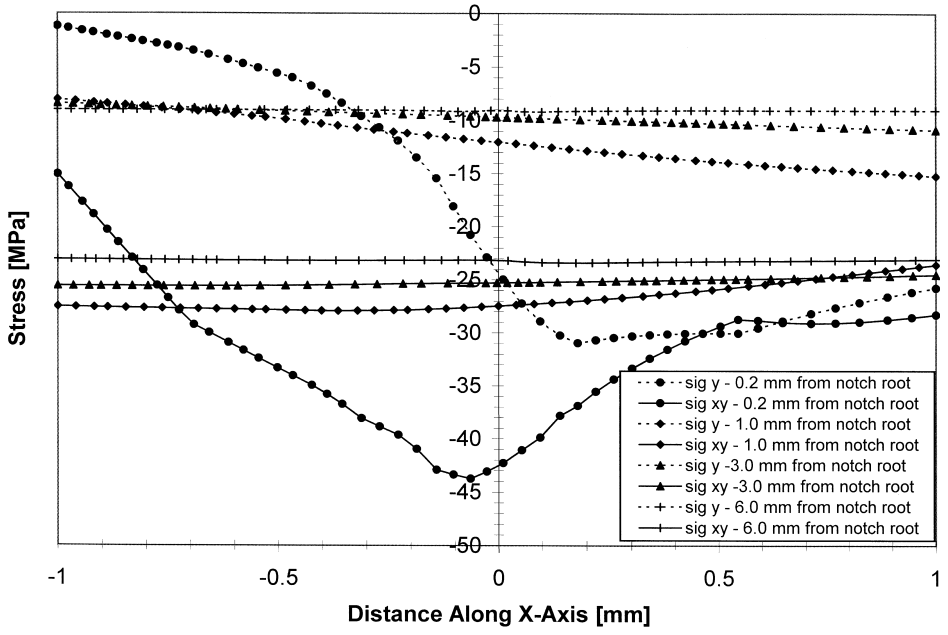

Fig. 25. Stresses parallel to the x axis near the notch-root for the Iosipescu model with notch-root splits.

intralaminar damage zone (2) are not easily observed visually. To overcome the difficulties in detecting the intralaminar damage zones (2) in non-transparent composite specimens, ultrasonic techniques were used in this research to generate images of the damage zones in carbon-fibre/epoxy Ciba-Geigy XAS/914 Iosipescu specimens. The ultrasonic image presented in Fig. 26 clearly shows the location and size of the intralaminar damage zones. In particular, type 2 damage can be clearly seen on the left side of the notch-root axis (on the side opposite to the inner loading block). In addition, a notch-root split (1) and one internal axial crack (3) underneath the notch-root can also be observed.

Neither the crush zones (4) nor the axial splits near the notches (1) is associated with the intralaminar shear-failure process. However, the intralaminar damage zones (2) and axial cracks (3) are caused by the local biaxial shear dominated stresses in the specimen gage section. It can be seen from the numerical data in Figs. 24 and 25, that the stress distribution in the specimen without the notch-root splits is biaxial with large shear and transverse tensile stresses on the left side of the notch-root axis. For the specimen with the notch-root splits, the stress field on both sides of the notch-root axis is always shear/transverse compression with the compressive stresses on the left side lower than on the side of the inner loading block. The data in Figs. 24 and 25 clearly demonstrate that the intralaminar failure process in the specimen gage section before the onset of the notch-root splits has to be controlled by shear and transverse tension. After the split formation, the failure process in this region should be controlled by shear and transverse compression. It can be expected that the formation of intralaminar cracking along the fibers under the shear/transverse tension condition should be significantly easier than under the shear/compression condition. Significantly longer cracks should be formed in a unidirectional composite under shear/transverse tension than under shear/transverse compression conditions since their propagation along the fibers will be more restricted in the presence of large compressive transverse stresses. Therefore, the axial cracks in the specimen gage section (type 3) are most likely caused by the local shear/transverse tension stresses in the specimens before the notch-root splitting occurs which propagate after the splitting as a result of the sudden increase of the normal compressive stresses along the fibers (see Fig. 21). The intralaminar damage zones near the notches (type 2) are generated by the local shear/transverse

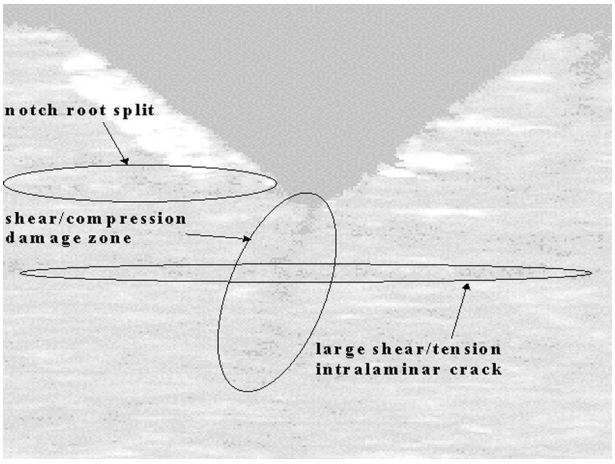

Fig. 26. Ultrasonic C-scan image of the notch-root area of a carbon-fibre/epoxy Iosipescu specimen.

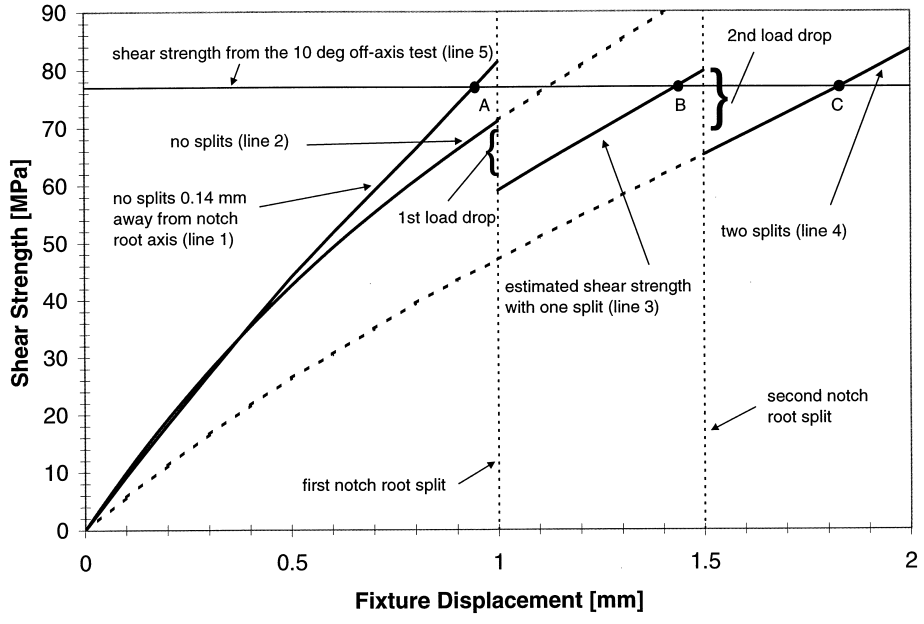

Fig. 27. Shear strength lines for the models with and without notch-root splits calculated over a 2-mm fixture displacement.

compression stresses near the notches in Iosipescu specimens with notch-root splits. Since the axial notch-root split formation process (type 1) at the notches is unpredictable, the relationships between the loads for the initiation of notch-root splits (1), axial cracks (2), and damage zones (3) cannot always be systematic.

Knowing the actual shear-strength data (77.0 MPa) from the 10° off-axis tests from the highest available loads at failure for the carbon-fibre/epoxy composite in conjunction with the fully nonlinear model of the Iosipescu test, an attempt was made in this research to predict the onset of the intralaminar failure in the gage section of the 0° Iosipescu specimens. If the stress fields in the immediate vicinity of the notch-roots are examined (see Figures 21–23) from the non-linear finite element models of the Iosipescu specimens with and without notch-root splits, it can be seen that the shear stresses are concentrated in these areas, with the highest shear stresses about 0.07 mm from the roots of the notches. Moreover, the transverse normal stresses in the uncracked specimen are tensile near the notches on the opposite side of the inner loading block (see Fig. 24). After splitting, the normal transverse stresses become compressive in this area (Fig. 25). Therefore, the intralaminar damage has to be initiated very close to the roots of the notches because of the combined effect of the maximum shear stresses and the corresponding transverse normal compressive stresses. Since the notch-root splits cannot be considered as the intralaminar shear failure mode in the specimen, the load at which intralaminar damage in the gage section initiates (either 2 or 3) has to be used to determine the actual shear strength of the composite.

In Fig. 27, shear strength lines obtained from the Tsai–Wu failure criterion [36] and the concentrated stress fields near the roots of the notches (considering all stress components) calculated from the non-linear models with and without the notch-root splits are plotted as a function of applied displacement. The numerical stress components and the composite strength values were used to extract the shear strength for each displacement increment. Shear strength line 1 was determined from the uncracked model (assuming that the intralaminar failure of the specimen is caused by the shear and transverse tensile stresses near the notches as shown in Fig. 24). The failure criterion was used at 0.14 mm from the notch-root axis on the side of notch-root split in the shear/transverse tension field for a displacement of 1 mm. This distance was selected since the probability of intralaminar failure at this point seems to be the largest as determined by the Tsai–Wu failure criterion [36] (see Fig. 28). Strength lines 2 (specimen without notch-root splits) and 4 (specimen with notch-root splits) in Fig. 27 were determined at the points along the notch-root axis where the shear stresses were maximum (approximately 0.07 mm from the notch-root along the notch-root axis). In these two cases, the intralaminar failure process was assumed to be caused by the highest shear stresses and the corresponding transverse compressive stresses along the notch-root axis.

After the first notch-root split, the stresses at the roots of the notches will be slightly relaxed with more stress relaxation expected to occur at the root with the split. Since the numerical stress data for the case with one split are not available, a shear-strength line (line 3) was

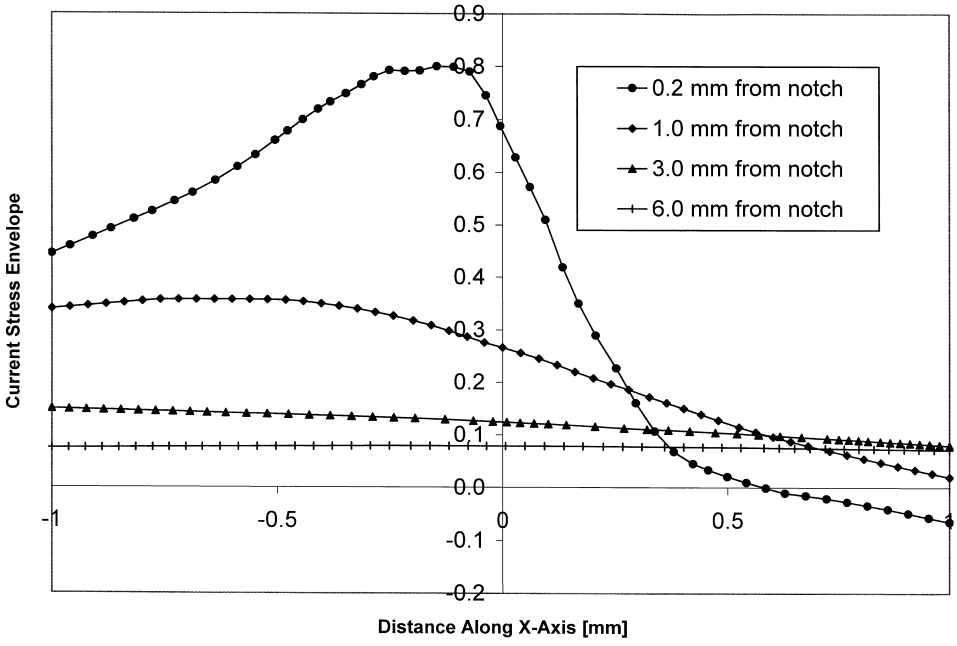

Fig. 28. Current stress envelope calculated using the Tsai–Wu failure criterion [36] for the specimen without notch-root splits.

subsequently estimated assuming that the notch-root splits are of equal lengths and the shear-strength reduction for one split is half of the total reduction for two splits (average of lines 1 and 4).

The horizontal line (line 5) in Fig. 27 represents the highest shear strength of the composite obtained from the 10° off-axis tests and the non-linear numerical model of the test. if the shear strength from the 10° off-axis experiments is taken as the true shear strength of the composite, the onset of the shear intralaminar damage in the Iosipescu specimens can be predicted by examining the data in Fig. 27. Whenever a shear strength line (either 1, 2, 3 or 4) crosses the shear strength line determined by the 10° off-axis tests (line 5) a biaxial shear-dominated intralaminar failure process should occur.

It can be seen from Fig. 27 that the shear strength line 1 is above lines 2, 3, and 4. Moreover, this particular line crosses line *5* (point A) sooner than lines 2, 3, and 4 and the intersection point is just before the first notch-root split. Therefore, the condition for intralaminar failure is satisfied for the uncracked specimen at this particular point (point A) and the failure process should be controlled by shear and transverse tension. However, this is only true if line 5 is determined accurately and the displacement for the first notch-root split is higher than the displacement for point A.

Line 2, determined from the numerical model without the notch-root splitting, does not cross line 5 before the first split. Therefore, the initiation of the intralaminar damage as a result of maximum shear and compression in the gage section of this particular specimen is impossible. It can be seen that line 3 (the estimated line for a model with one notch-root split) intersects line 5 (at point B) just before the second split is initiated. Therefore, the initiation of the intralaminar shear damage as a result of maximum shear and compression near the notch-root should occur just before the second notch-root split (for this particular specimen), on the side of the specimen with the single notch-root split. However, the intralaminar shear/compression damage process cannot be continuous. After the second split, the shear strength line of the composite (line 4 from the model with two axial splits) is again below line 5 following some stress relaxation. Thus, the intralaminar failure process has to be arrested until the stresses are again high enough to reinitiate the failure process. The intersection point between lines 4 and 5 (point C) indicates the reinitiation of the intralaminar shear/compression damage propagation after the second split.

The comparison between the 10° off-axis and Iosipescu tests as presented in Fig. 27 in terms of the shear-strength lines evaluated from the stresses is not always straightforward, however. The notch-root splits are formed as a consequence of the local normal and shear-stress concentrations on the surfaces of the notches and the loads for the notch-root split initiation are strictly related to the notch geometry, local damage caused by machining, and the overall strength properties of the composite material. Therefore, they can occur unpredictably at different loads for any given composite material. However, they can affect the interpretation of the shear strengths of the composite material evaluated from the Iosipescu test. Depending on the loads at notch-root splitting, either shear/transverse tension or shear/transverse compression intralaminar damage will be formed in 0° Iosipescu specimens. If the loads at splitting are low, below the load for point A, the shear/compression mode of failure (type 2) will occur and the shear/tension cracks should not be observed. For high loads at splitting (if the first notch-root split occurs above point A) the shear/tension mode of failure (type 3) should occur. The shear/tension cracks, however, will be affected by the notch-root split formation. Since notch-root splitting increases significantly the axial compressive stresses along the fibers the shear/tensile cracks should be able to propagate further along the fibers at some stages of loading after the notch-root splitting providing that the increases in the transverse compressive stresses are overcome.

The evaluation of the shear strength of a composite by means of the Iosipescu shear test can be quite difficult, as shown above. Perhaps this is the reason why so much confusing data have been published in the past regarding the relationship between the loads at splitting and the initiation of intralaminar shear-dominated damage in the gage sections of 0° Iosipescu specimens.

5.4. Strains in the 10° off-axis and Iosipescu specimens

5.4.1. 10° off-axis test

In Table 2, the strains in the 10° off-axis specimen determined analytically and from the linear/elastic and elastic/plastic models are presented. The strains were determined for a load of 27 kN (which is the highest load at failure for the carbon-fibre/epoxy material). It can be seen that the shear strains at failure for a load of 27 kN (calculated from the numerical strain gages) were $\gamma_{12} = 0.91\%$ and $\gamma_{12} = 1.38\%$ for the linear/elastic and elastic/plastic models, respectively. The analytical

Table 2
Strains in the 10° off-axis test calculated numerically and analytically

	Analytical (%)	Numerical (%)	
		Linear/elastic	Elastic/plastic
ε_{11}	0.296	0.290	0.293
ε_{22}	0.0006	−0.014	0.0009
γ_{12}	1.192	0.914	1.380

approach provided the shear strain somewhere between the strains from the two numerical models. Balakrishnan et al. [22] did not report any shear strain values in their 10° off-axis tests; therefore, there is no experimental comparison for the above numerical and analytical values. It was observed in the numerical models that all three strain components were relatively uniform throughout the gage section of the specimen. Similar to the stress fields in Table 1, the strain fields in the fiber coordinates are also biaxial.

5.4.2. Iosipescu test

Figs. 29–31 show that the strain components along the notch-root axis of the Iosipescu specimen are not uniform for both non-linear models with and without notch-root splits. In fact, the strain concentrations at the notch-root are in general larger than the corresponding stress concentrations. However, the splits significantly reduce the shear-strain concentration near the roots of the notches. As far as the normal strains along the notch-root axis (ε_{22}) are concerned, splitting

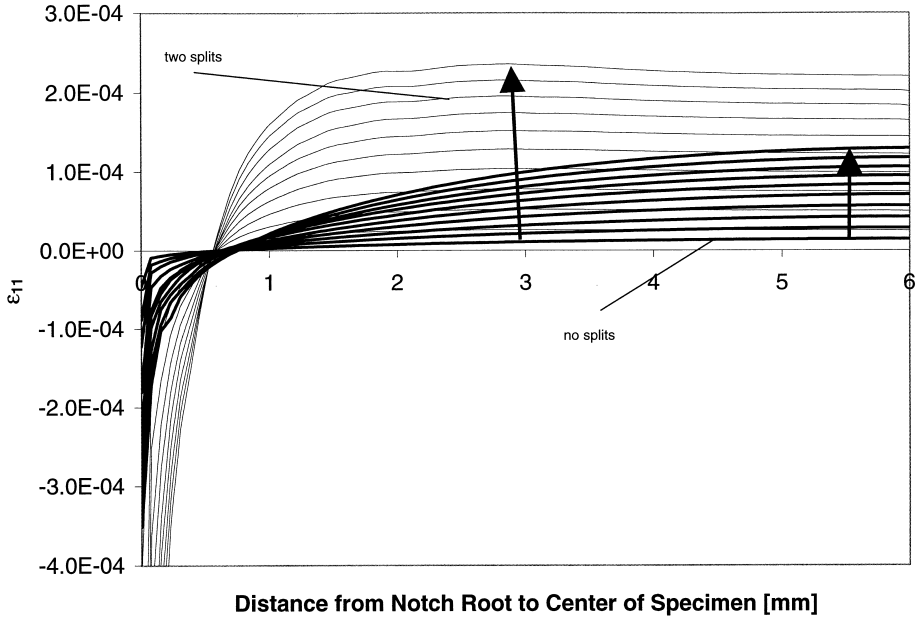

Fig 29. Normal strain (parallel to fibers) plotted along the notch-root axis over 10 sub-steps for Iosipescu models with and without axial splitting. Progressive loading is indicated.

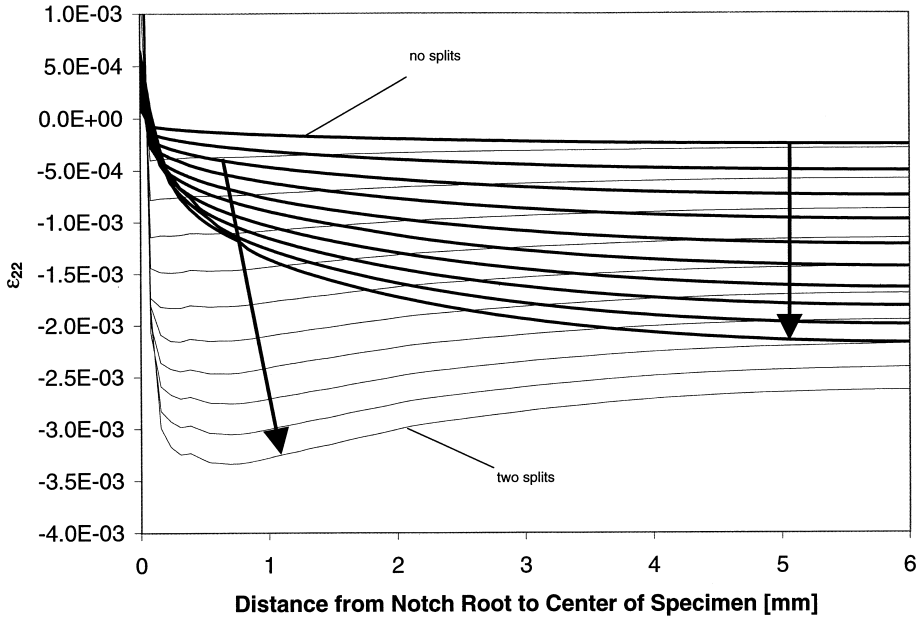

Fig. 30. Normal strain (perpendicular to fibers) plotted along the notch-root axis over 10 sub-steps for Iosipescu models with and without axial splitting. Progressive loading is indicated.

increases the strains with their maximum values occurring approximately 0.5 mm from the roots of the notches which does not correspond to the location of the maximum shear strain. The normal transverse strain decreases to zero approaching the notch-root.

It can be seen from Fig. 31 that the shear strain at the center of the specimen is 0.513% and the maximum near the notch-root is 0.659% for the same 1 mm displacement from the model with two notch-root splits. Therefore, there is about a 28% discrepancy between the shear strains at the specimen center (where the strain gage is located) and the largest shear strain near the notch-root. For the non-linear model without the splits, the shear strain at the center is 0.493% whereas the largest shear strain at the notch-root is 1.067%.

5.4.3. Comparison of the tests in terms of strains

It has been shown that the criterion for intralaminar failure (either shear/tension or shear/compression) is satisfied in terms of stresses at failure at point A and point C in Fig. 27. At these two points the shear-strength lines in the uncracked and axially cracked Iosipescu specimens match the shear strength lines in the 10° off-axis test. In this section, strains in the two Iosipescu models will be compared with the strains at failure in the 10° off-axis test.

At point A, the experimentally determined shear strain γ_{12} in the specimen gage section (see Fig. 14) was found to be 0.6%. Obviously, the maximum shear strain near the notches could not be determined experimentally. However, from the Iosipescu model without the notch-root splits the ratio between the maximum shear strain near the notch and the average shear strain at the center could be computed. It was found that the ratio was almost 2 with the strain near the notches twice the shear strain at the center. The corresponding normal strain ε_{22} for the maximum γ_{12} was $+0.007\%$. If the maximum shear strain along the notch-root axis (1.2%) for the model without notch-root splits is compared to the shear strain at failure from the 10° off-axis experiment (1.38%), it can be seen that the shear strain at point A from the Iosipescu model is slightly lower than from the 10° off-axis test. However, it has been determined that the transverse normal strains in the 10° off-axis and Iosipescu specimen (without splits) are $+0.0009\%$ and $+0.007\%$, respectively. Therefore, even though shear strain is lower in the uncracked Iosipescu specimen, the higher transverse tensile strains will make the intralaminar shear/tension failure easier even for slightly lower shear strains.

At point C, the shear strains from the 10° off-axis test, numerically determined maximum shear strain near the notch-root from the Iosipescu model with two notch-root splits, and the experimental shear strains (with numerical correction to account for the local strain concentration at the notches as discussed above) are 1.38, 1.18, and 1.74%, respectively. In this case, the agreement between the numerical Iosipescu model and the 10° off-axis test is still quite good. The discrepancy between the experiment and the numerical Iosipescu strains is a consequence of three effects that were not modeled numerically, namely the crushing (cracks in the crush zones were not considered), the shear/tension intralaminar crack, and the shear/compression damage zones. If the stress relaxation caused by these factors were numerically modeled, then the shear-strength lines

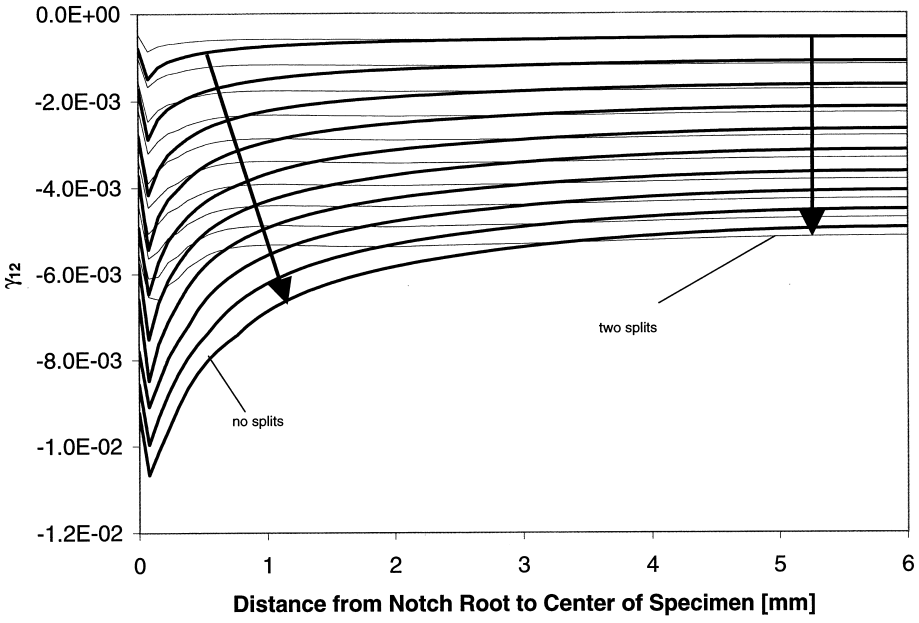

Fig. 31. Shear strain plotted along the notch-root axis over 10 sub-steps for Iosipescu models with and without axial splitting. Progressive loading is indicated.

(line 3 and 4) would cross the 10° off-axis shear-strength line (line 5) at higher displacements, which would increase the numerical Iosipescu shear-strain value given above. Considering the obvious limitations of the non-linear Iosipescu models, it is not surprising that the experimental strains are higher than the strains from the 10° off-axis and the numerical model. However, the above three effects did not affect the analysis of strains before the initiation of notch-root splits.

Since point B for lines 3 and 5 in Fig. 27 was only estimated and the strain values for a single notch-root split model are not available, the Iosipescu and 10° off-axis tests cannot be compared at this point with respect to strains.

5.5. Explanation of failure of unidirectional Iosipescu specimens

The purpose of this research was finally to clarify the confusion regarding the application of the Iosipescu test as recommended by ASTM standard (D 5379-93) for the shear-strength measurements of unidirectional composites. The standard says "In $[0]_n$ specimens tested in the 1–2 plane, a visible crack typically develops at the notch-root, causing a small load drop prior to ultimate failure. The small load accompanying the notch-root crack is not considered the failure load: rather the load that accompanies failure in the test section shall be used as the failure load." The problem is that the standard does not indicate which failure in the test section should be considered as the shear failure. It has been shown in this research that the intralaminar shear/tension failure near the roots of the notches before notch-root splitting and the shear/compression failure after the formation of the axial splits can be taken as the predominantly shear failure mode in unidirectional Iosipescu specimens. This has been accomplished by performing very detailed non-linear finite-element computations of the test considering the actual non-linear behavior of the composite material. Very close agreements between the shear failure of a unidirectional carbon-fibre/epoxy composite obtained from two independent tests (10° off-axis and unidirectional Iosipescu) have been achieved in terms of stresses and strains. It has been shown that the shear strength determined from the Iosipescu test closely matches the strength determined from the 10° off-axis experiments.

The shear failure of unidirectional 0° Iosipescu specimens is associated with the formation of either axial cracks in the gage section near the notches of the specimen before the formation of notch-root splits due to shear/tension or small intralaminar shear/compression damage zones which propagate from the roots of the notches slightly away from the notch-root axis after the formation of notch-root splits. The shear/tension cracks should form near the notches in the specimens without notch-root splits just before the initiation of the first split (at point A in Fig. 27). After notch-root splitting the most favorable intralaminar failure process near the notch-root with the split is the formation of the shear/compression damage zones near the notch (points B and C in Fig. 27). Since shear/compression damage is much more difficult to form than shear/tension damage because of the higher compressive transverse strength than the transverse tensile strength and the closing of micro-cracks in compression, it could be expected that the length of intralaminar cracks caused by shear/tension should be significantly larger than the size of cracks caused by shear/compression. Therefore, the damage zones (2 in Fig. 2) consisting of short cracks along the fibers must be formed under the shear/compression conditions either between the axial splits (at the notch with splitting) or above the second split. The much longer cracks in the gage section beneath the notch-root (3 in Fig. 2) must be generated due to the combined effect of the shear and transverse tension stresses and their subsequent propagation will be affected by the notch-root split formation. However, axial cracks near the notches can also occur after the first split at the notch without the notch-root split.

It has been shown by Kumosa and Hull [13] that the intralaminar damage zones (2 in Fig. 2) propagate in the direction slightly way from the notch-root axis on the sides of the axial splits. This can also be seen in Figs. 3 and 4. Also, the shear/tension cracks are located underneath the notch-root on the side of the notch-root split. The directions of the damage-zone propagation and the location of shear/tension crack initiation can be explained by examining the local stress distributions near the notches from the fully non-linear numerical models with and without notch-root splits (see Figs. 24 and 25). It can also be seen in Fig. 25 that the amount of compression near the notch on the side of the notch-root axis with the notch-root splits is lower than on the side of the loading block. That is the reason why the shear/compression zones propagate on this side of the specimen. The propagation of the shear/compression zones becomes more difficult towards the specimen center since the shear and compressive stresses decrease significantly in this direction for a given applied displacement (see Fig. 25).

The initiation of the shear/tension cracks (3 in Fig. 2) must occur also on the side of the specimen with the notch-root split before the split initiation since the normal stresses on the inner block side are compressive (see Fig. 24). Their initiation further away from the notch-root towards the specimen center is more difficult since the magnitudes of the shear and transverse tensile stresses in this direction decrease for a given displacement.

The interpretation of the intralaminar shear dominated failure process in the 0° Iosipescu specimens as shown in Fig. 27 will be changed if the splits occur at

other loads. There are several possible combinations of the initiation of type 2 and type 3 cracking depending on loads at notch-root splitting and the overall strength properties of the unidirectional composite material. Moreover, if crushing is significant at low loads it will also significantly affect the stress distributions in either specimen with or without notch-root splits and thus the final determination of the shear strength.

The proposed non-linear failure model of 0° unidirectional Iosipescu specimens has its limitations. In particular, the effect of crushing near the loading blocks on the stress distributions was not adequately addressed. The plastic deformation of the composite within the crush zone was modeled without considering the presence of either interlaminar or intralaminar cracks within the zones. These cracks (if present) must further relax the overall stresses in the specimens. In addition, the presence of the shear/tension cracks and shear/compression damage zones in the gage section was also not considered in the non-linear models of the specimens. Finally, the proposed model of failure in the 0° unidirectional carbon-fibre/epoxy Iosipescu specimen is only true if the shear strength of the composite is accurately determined from another test. In this particular case, the highest available shear strength data for the composite from the 10° off-axis test were employed to explain the intralaminar failure process in the Iosipescu specimens.

If the Iosipescu shear test is used for the shear-strength determination of unidirectional composites the damage at the roots of the notches and its relation to the split formation and the initiation of significant crushing should be continuously monitored. The stress field for the specimen (with the correct non-linear material properties for the composite) must then be determined numerically. The problem is that intralaminar failure is very difficult to monitor during testing, especially in non-transparent unidirectional composites. Also, the actual nonlinear material behavior must be determined using other tests (for example the 10° off-axis test). This makes the Iosipescu shear test very difficult and almost impractical if applied for the shear strength determination of unidirectional composites.

6. Conclusions

1. It has been shown in this research that the 10° off-axis and Iosipescu shear tests can be successfully used to determine the shear-strength properties of unidirectional composites. This can only be accomplished if fully non-linear finite-element computations of the tests are performed which take into account the actual non-linear material behavior of a unidirectional composite. In particular, the Iosipescu shear test must be modeled with three non-linearities, namely boundary contact, geometric, and material non-linearities.

2. The stresses and strains at failure for the Iosipescu and 10° off-axis tests are in almost perfect agreement if either the fully non-linear models of the Iosipescu specimen with or without axial splits are used. This is determined by the relationship between the notch-root split formation and the initiation of intralaminar damage zones (either type 2 or type 3) at the roots of the notches. If the damage zones are formed above the second notch-root split the non-linear model with two axial splits should be used. However, if the intralaminar damage at the notch-root occurs before the initiation of the first notch-root split the non-linear model without splits should be used. In the case of the damage occurring between the splits the shear strength can be approximated by using the average of the two models. In either case the obtained shear strength results should be verified and compared with another shear test for unidirectional composites. The 10° off-axis test could be used for this purpose only if a significant number of tests are performed. The highest loads at failure then should be used to determine the shear strength. This will potentially minimize severe effects of specimen machining and gripping, especially in the case of very brittle composites.

3. To obtain the shear strength of a unidirectional composite with the Iosipescu shear test the intralaminar damage near the roots of the notches should be continuously monitored during testing. The critical loads for the initiation of the damage with respect to the loads at splitting should be determined. Then, an appropriate finite-element model should be used to determine the stresses and strains at failure near the roots of the notches. The first intralaminar crack to form very close the notch-root should be considered for the shear strength determination. Since the stress fields in this area are always biaxial, a multi-axial failure criterion should be used to extract the actual shear strength.

Acknowledgements

This research was supported by the National Science Foundation under grant CMS-9696160. The authors would like to thank W.N. Cobb of the University of Denver Research Institute for his help in obtaining Fig. 26.

References

[1] Swanson SR, Messick M, Toombes GR. Comparison of torsion tube and Iosipescu in-plane shear test results for a carbon fibre-reinforced epoxy composite. Composites 1985;16(3):220–4.
[2] Lee S, Munro M. Evaluation of in-plane shear test methods for advanced composite materials by the decision analysis technique. Composites 1986;17(1):13–22.
[3] Pierron F, Vautrin A. The 10° off-axis tensile test: a critical approach. Composites Science and Technology 1996;56:483–8.

[4] Adams DF, Lewis EQ. Experimental assessment of four composite material shear test methods. Journal of Testing and Evaluation 1997;25(2):174–81.
[5] Iosipescu N. New accurate procedure for single shear testing of metals. Journal of Materials 1967;2(3):537–66.
[6] Adams DF, Walrath DE. Iosipescu shear properties of SMC composite materials. In: Composite materials: testing and design (Sixth Conference) (ASTM STP 787). Philadelphia: ASTM, 1982. p. 19–33.
[7] Adams DF, Walrath DE. Further developments of the Iosipescu shear test method. Experimental Mechanics 1987a;27(2):113–9.
[8] Adams DF, Walrath DE. Current status of the Iosipescu shear test method. Journal of Composite Materials 1987b;21:494–507.
[9] Walrath DE, Adams DF. The Iosipescu shear test as applied to composite materials. Experimental Mechanics 1983;23(1):105–10.
[10] Barnes JA, Kumosa M, Hull D. Theoretical land experimental evaluation of the Iosipescu shear test. Composites Science and Technology 1987;28:251–68.
[11] Broughton WR, Kumosa M, Hull D. Analysis of the Iosipescu shear test as applied to unidirectional carbon-fiber reinforced composites. Composites Science and Technology 1990;38:299–325.
[12] Ho H, Morton J, Farley GL. Non-linear numerical analysis of the Iosipescu specimen for composite materials. Composites Science and Technology 1994;50:355–65.
[13] Kumosa M, Hull D. Mixed-mode fracture of composites using Iosipescu shear test. International Journal of Fracture 1987;35:83–102.
[14] Morton J, Ho H, Tsai MY, Farley GL. An evaluation of the Iosipescu specimen for composite materials shear property measurement. Journal of Composite Materials 1992;26(5):708–50.
[15] Odegard G, Kumosa M. Elasto-plastic analysis of the Iosipescu shear test. Journal of Composite Materials 1999;33(21):1981–2001.
[16] Odegard G, Searles K, Kumosa M. A critical examination of the Iosipescu shear test as applied to 0° unidirectional composite materials. Mechanics of Composite Materials and Structures 1999;6(3):229–56.
[17] Pierron F, Vautrin A. Measurement of the in-plane shear strength of unidirectional composites with the Iosipescu test. Composites Science and Technology 1997;57:1653–60.
[18] Kumosa M, Han Y. Non-linear finite element analysis of Iosipescu specimens. Composites Science and Technology 1999;5:561–73.
[19] Chamis CC, Sinclair JH. Ten-deg off-axis test for shear properties in fiber composites. Experimental Mechanics 1977;17(9):339–46.
[20] Pindera MJ, Herakovich CT. Shear characterization of unidirectional composites with the off-axis tension test. Experimental Mechanics 1986;26(1):103–12.
[21] Sun CT, Chung I. An oblique end-tab design for testing off-axis composite specimens. Composites 1993;24(8):619–23.
[22] Balakrishnan MV, Bansal B, Kumosa M. Biaxial testing of unidirectional carbon–epoxy composite using biaxial Iosipescu test fixture. Journal of Composite Materials 1997;31(5):486–508.
[23] Hill R. A theory of the yielding and plastic flow of anisotropic metals. In: Proceedings of Royal Society of London, London, 1948. p. 281–97.
[24] Griffin OH, Kamat MP, Herakovich CT. Three dimensional inelastic finite element analysis of laminated composites. Journal of Composite Materials 1981;15:543–60.
[25] Spencer AJM. Plasticity theory for fibre-reinforced composites. Journal of Engineering Mathematics 1992;26:107–18.
[26] Sun CT, Chen JL. A simple flow rule for characterizing nonlinear behavior of fiber composites. Journal of Composite Materials 1989;23(10):1009–20.
[27] Hansen AC, Blackketter DM, Walrath DE. An invariant-based flow rule for anisotropic plasticity applied to composite materials. Journal of Applied Mechanics 1991;58(4):881–8.
[28] Chen JL, Sun CT. A plastic potential function suitable for anisotropic fiber composites. Journal of Composite Materials 1993;27(14):1379–90.
[29] Zhao YH, Weng GJ. Theory of plasticity for a class of inclusion and fiber-reinforced composites. In: Micromechanics and inhomogeneity: the Toshio Mura 65th Anniversary Volume. New York: Springer-Verlag. 1990.
[30] Voyiadjis GZ, Thiagarajan G. An anisotropic yield surface model for directionally reinforced metal-matrix composites. International Journal of Plasticity 1995;11(8):867–94.
[31] Mendelson A. Plasticity: theory and application. New York: Macmillan, 1968.
[32] Spencer AJM. Theory of invariants. In: Continuum physics vol. I. New York: Academic Press, 1971. p. 240–353.
[33] Bansal A, Kumosa M. Experimental and analytical studies of failure modes in Iosipescu specimens under biaxial loadings. Journal of Composite Materials 1995;29(3):334–58.
[34] Odegard G, Searles K, Kumosa M. Non-linear analysis of woven fabric-reinforced graphite/PMR-15 composites under shear-dominated biaxial loads. Mechanics of Composite Materials and Structures 2000;7(2):129–52.
[35] Adams DF, Lewis EQ. Experimental strain analysis of the Iosipescu shear test specimen. Experimental Mechanics 1995;35(4):352–60.
[36] Tsai SW, Wu EM. A general theory of strength for anisotropic materials. Journal of Composite Materials 1971;5:58–80.
[37] ASM Committee on Forms and Properties of Composite Materials. High-strength medium-temperature thermoset matrix composites. In: Composites, engineered materials handbook, vol. 1. Metals Park (OH): ASM International, 1987. p. 399–415.